CHAPTER 3

SMARTPHONE BASED SPECTROSCOPIC SENSING FOR ESTIMATION OF PH LEVEL AND TOXIC METAL IONS IN SOIL

This chapter outlines the development of a spectroscopic based sensing platform using a smartphone. The developed sensor has been utilized for estimation of pH level in soil. The importance of monitoring pH value in soil is also included in the chapter. Further, the applicability of the developed sensor has been demonstrated for localized surface plasmon resonance (LSPR) based sensing. The quantitative estimation of two metal ions namely arsenic and lead in soil using the synthesized gold nanoparticles on a smartphone platform has been discussed. The feasibility of the developed sensing platform has been verified by comparing the experimental results with laboratory-grade tool.

3.1 Introduction

In agriculture, the pH value of soil determines the yields of good quality crops. Soil pH is a critical parameter for all chemical and biological processes [1]. The pH value of soil provides information not only about its acidity or alkalinity but also on metal solubility, nutrient availability, and microorganism activity [2, 3]. A small change in pH value (± 0.1 units) can affect the soil's biological or chemical process [4]. Thus, a precise estimation of pH value in soil is essential to improve the productivity and management of agricultural farmland. Different techniques, such as colorimetric, spectrometric, electrochemical, are available to measure the soil's pH value [5]. Conventional methods of soil pH measurement, such as glass electrodes, have some inherent limitations [6]. For instance, the existence of asymmetry potentials in the

electrode junction may result in an error in pH value [7, 8]. Both colorimetric and spectrometric methods involve pH-sensitive dye. Earlier, the soil pH measurement was done by adding a single pH indicator dye or a mixed indicator dye into soil extracts, and the developed color was compared visually to a standard color chart [9, 10]. The colorimetric method has a very low accuracy (±0.5 pH units) due to the usage of standard color charts. Again, the spectrometric methods require optical tools that are bulky, costly, and, in general, are laboratory-confined [11–13].

Again, heavy metal contamination in agricultural soils is a significant environmental issue that adversely affects the crop development and human health which might enter to our body through the food chain. The contamination of heavy metals in soil is primarily increased by chemical waste from industries, and the exploitation of chemical fertilisers and pesticides. Arsenic (As) is one of the toxic elements present in water and soil which has dangerous impacts on human life [14]. It has four potential oxidation states (3, +3, 0, and +5) out of which As(III) is considered as the most hazardous one due to its carcinogenic tendency [15]. Consumption of As(III) could lead to various diseases like peripheral vascular disorder, keratosis, diarrhea, abdominal pain and different types of cancer etc. [16–18]. Lead (Pb) is another toxic heavy metal present in the crust of the earth, water, and soil that may possibly harm every system in the human body, including the reproductive, nervous, hematopoietic, hepatic, and renal systems [19, 20]. Due to the harmful impacts of As and Pb in human health, monitoring of these toxic pollutants present in different sources is of utmost importance. Different regulatory organisations have issued permissible limit for certain toxic pollutants in water and soil medium. The world Health Organization (WHO) has set the limit for As as 10 ppb in drinking water [21]. The Environmental Protection Agency (EPA) has set a hazardous limit for Pb in drinking water as 15 ppb [22]. As(III) is mostly found in soil medium contaminated from waste water. Although geographical differences affect the amount of As(III) present in soils, the average As value present in soil is 5 mg/kg i.e. 5 ppm [23]. Naturally, low quantities of Pb are present in soil. The amount of Pb present in agricultural soil ranges between 15 and 40 ppm [24]. Therefore, it is crucial to identify As(III) and Pb(II) in soil to prevent these pollutants from entering into the food chain.

In this chapter, the development and application of smartphone as a spectrometric sensing tool has been demonstrated for detection of pH value and toxic metal ions in soil. In the first part of the chapter, design of the spectrometric sensing tool on a smartphone platform has been demonstrated. The transmission signal intensity of captured by the rear camera of the smartphone has been utilized for spectrometric based sensing of pH value in soil. In the next phase, the applicability of the designed spectrometric sensing tool has been explored for localized surface plasmon resonance (LSPR) based detection of hazardous metal ions (arsenic and lead) present in soil.

The detailed methodology of estimation of the metal ions based on the LSPR shift of gold nanoparticles has been demonstrated in section 3.3 of the chapter.

3.2 Design of smartphone-based spectrometric sensor for accurate estimation of pH value in Soil

Considering the need of an alternative pH sensing tool, this section of the thesis describes the development of a spectrometric tool on a smartphone platform that is low-cost, robust, and easily portable to estimate pH value in soil with a good degree of accuracy and reliability. A 3D printed cradle has been developed to hold the optical components which can be attached easily to the phone as a plug and play device. The performance of the designed smartphone sensor has been compared with a laboratory-grade spectrometer. The designed tool has been successfully implemented while measuring the pH value of different field-collected soil samples. The various stages of developing the proposed smartphone spectrometric tool are described in the following subsections.

3.2.1 Materials and methods

3.2.2 Preparation of the standard solutions and reagents

To investigate the optical response over a wide range of pH values in the range 4 to 10, we choose a universal indicator dye (product no. Q38126) procured from Thermo Fisher Scientific India as a pH-sensitive dye. Buffer solutions of pH values 4, 7, and 9 (Merck, India) have been used as standard pH media. Also, buffer solutions of varying pH values of 5, 6, 8, and 10 were synthesized in the laboratory following the standard procedure [25]. Using a standard pH meter (Cyber Scan pH 700), all the seven samples were measured to ensure the correct pH values of the samples. 3mL each of the pH buffer samples has been treated with 60 µl universal indicator dye to get various colored pH media. The photo image of the universal dye treated standard pH samples is given figure 3.1.

3.2.3 Soil sample collection and extraction procedure

Six field-collected soil samples have been acquired from the Department of Environmental Science, Tezpur University to demonstrate the applicability of the proposed tool. The samples were collected from various locations of West Bengal, India. The soil samples were air-dried and sieved to obtain a size ($<$ 2-mm) for further use. Soil extracts were prepared from each soil in the ratio of 1:2.5 w/v (10 g soil/25

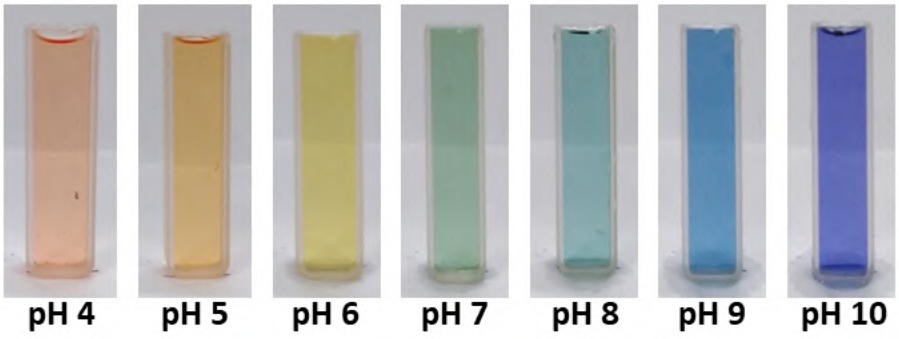

Figure 3.1: Photo images of cuvette containg standard pH samples in the pH range 4-10 treated with universal pH indicator dye.

mL water). The soil solutions were shaken for one hour on an orbital shaker to mix well, centrifuged at 2000 RPM for 30 min as per standard methods [26]. Following this step, 15 mL each of the soil extract supernatant was carefully pipetted into a clean test tube for further use. The pH value of each sample was investigated before the experiment using a commercially available pH meter. After this step, 3 ml of each soil sample has been treated with 60 µl of universal indicator dye for immediate spectrometric analysis.

3.2.4 Design of the sensing setup

Prior to designing of the sensing setup, the optical elements have been mounted in an optical breadboard and measured the focal length of the lenses for the precise alignment of the optical components. The measured data has been used to design the lens holders and adapters using a 3D modeling software- "ZW3D". The designed parts have been fabricated in a 3D printer- "Raise3D", having 10-Micron Layer Resolution. Using high resolution 3D printing technology, lens holder, sample holder and adapters with precise dimension can be fabricated. After fabrication, the optical components have been placed in exact measured position of the 3D printed holders and can be attached and aligned with each other in order to achieve a precise opto-mechanical alignment.The schematic of the proposed smartphone sensor is shown in figure 3.2(a). A broadband optical source having a tungsten halogen light from Ocean Optics (Model: LS-1) has been used in the present study, which emits wideband continuous wavelengths in the range 360-2000 nm. The light signal from a broadband optical source is allowed to pass through a pinhole of diameter 50 μm. The emerging light from the pinhole is collimated by using a collimator lens (7 mm diameter, Edmund Optics) of focal length 11 mm. The collimated light signal then passes through the sample placed in a quartz cuvette having a dimension 45 $\times$ 12.5 $\times$ 12.5 mm and an optical path length 10 mm. The transmitted light beam from the sample is received by a cylindrical lens (12.5 mm diameter, Edmund Optics) with a

focal length of 50 mm. The emergent light from the cylindrical lens is focused tightly into a line beam on a piece of DVD that acts as a transmission grating in the present set-up. The DVD grating disperses the line beam into its component wavelengths, which has been recorded by the imaging sensor of the phone. The reflective layer of the DVD has been removed by using an adhesive tape. The grating is placed at an angle of 47° to the direction of the incoming light so that the first-order diffraction spectrum is captured by the CMOS sensor (16 MP, 1920 × 1080 pixels) of the smartphone (Samsung Galaxy C9 Pro). Figure 3.2(b) shows the photo image of the proposed smartphone sensing set-up. The dispersed spectrum can be seen on the display panel of the smartphone. The dispersed spectrum image of a broadband optical source (Ocean Optics, Model: LS-1) collected from DVD based grating element is shown in figure 3.2(c). The broadband optical source emits wideband of continuous wavelengths in the range 360-2000 nm. But the phone camera sensor response is sensitive only in the wavelength range 400 nm to 700 nm due to the involvement of an infrared (IR) filter in the CMOS sensor chip, therefore, the captured dispersed spectrum consists of light intensity within the wavelength range 400-700 nm i.e. from blue to red as given in figure 3.2(c). The SEM image of the DVD grating is shown in figure 3.3. The track pitch of the DVD is measured to be 0.74 *mu* m or 1351 lines per mm. By using the standard formula [27], the angular dispersion or change in diffraction angle per unit wavelength of the grating of the first-order diffraction is calculated to be 0.00197 rad per nm. The dimension of the compact 3D printed optical set-up is measured to be 85 mm length, 30 mm breadth, and 30 mm height, and the weight is approximately 150g, excluding the smartphone.

3.2.5 Calibration of the device

At first, the dispersed spectrum of the broadband source, and two laser pointers green (529.5 nm) and red (652 nm) were recorded by the smartphone's camera. ImageJ, a freely available mobile app, has been used to determine pixel positions of the two laser sources. At first, the pixel intensity distribution along the pixels of the spectrum images of broadband and laser sources have been plotted by using the ImageJ software. The pixel positions of the laser sources have been determined from the pixel vs intensity plot. After this step, the pixel positions of these laser sources have been plotted with respect to their corresponding wavelength value. Thus the pixel based visible spectrum information recorded by the designed set up can be converted to wavelength scale. Figure 3.4 represents the pixel intensity distribution of the laser sources (green and red) along with the spectrum of broadband source measured by the designed smartphone sensing setup. For the designed optical set-up, the pixel positions for the red (652 nm) and green (529.5 nm) lasers are found to

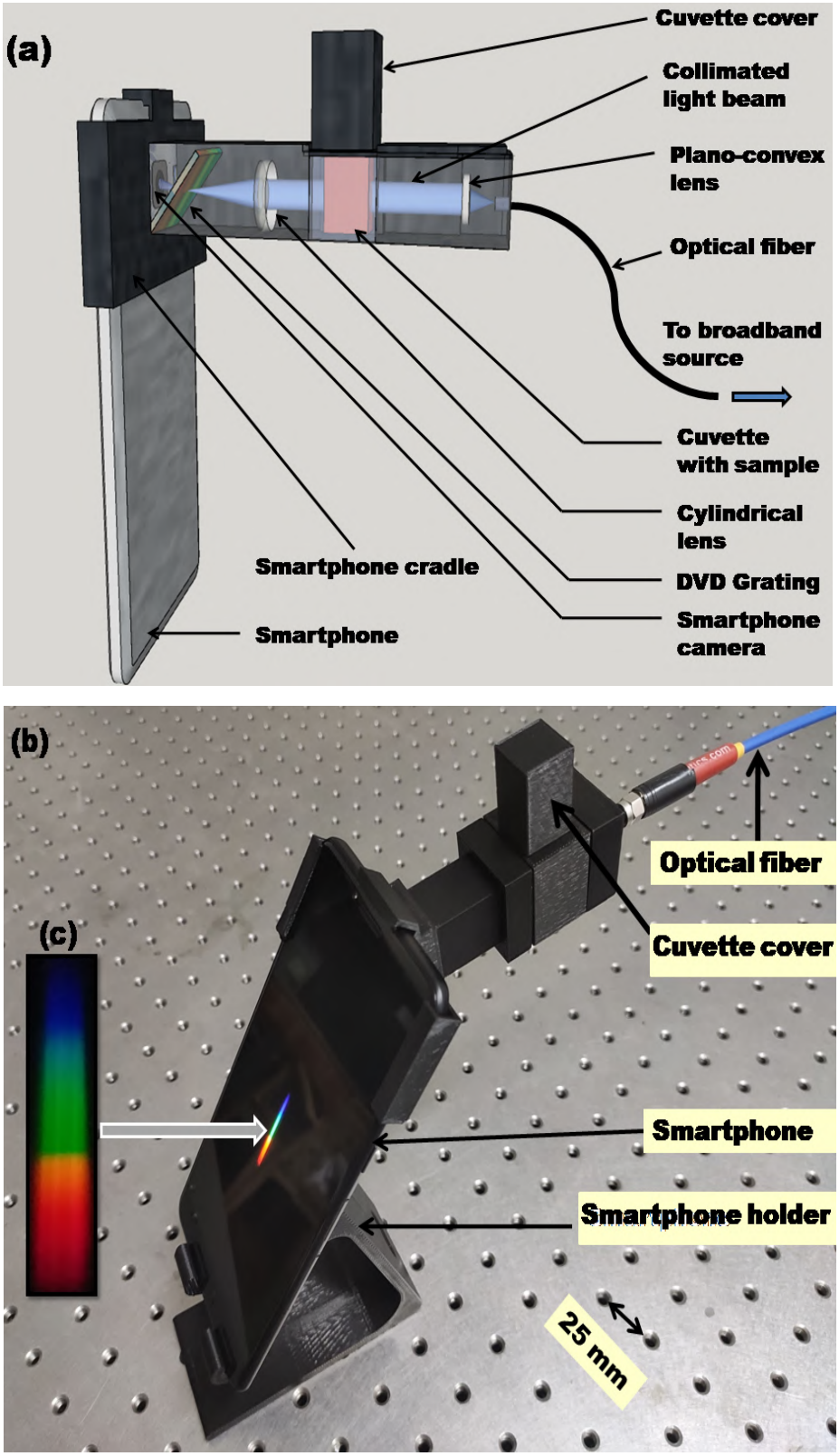

Figure 3.2: (a) Schematic of the smartphone-based sensor, (b) photo image of the designed sensor (c) cropped image of the bare spectrum taken by the designed sensor.

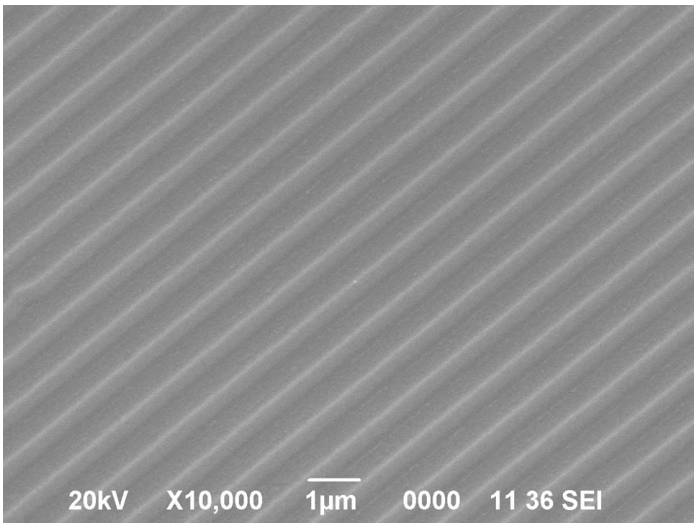

Figure 3.3: The SEM image of the used DVD grating.

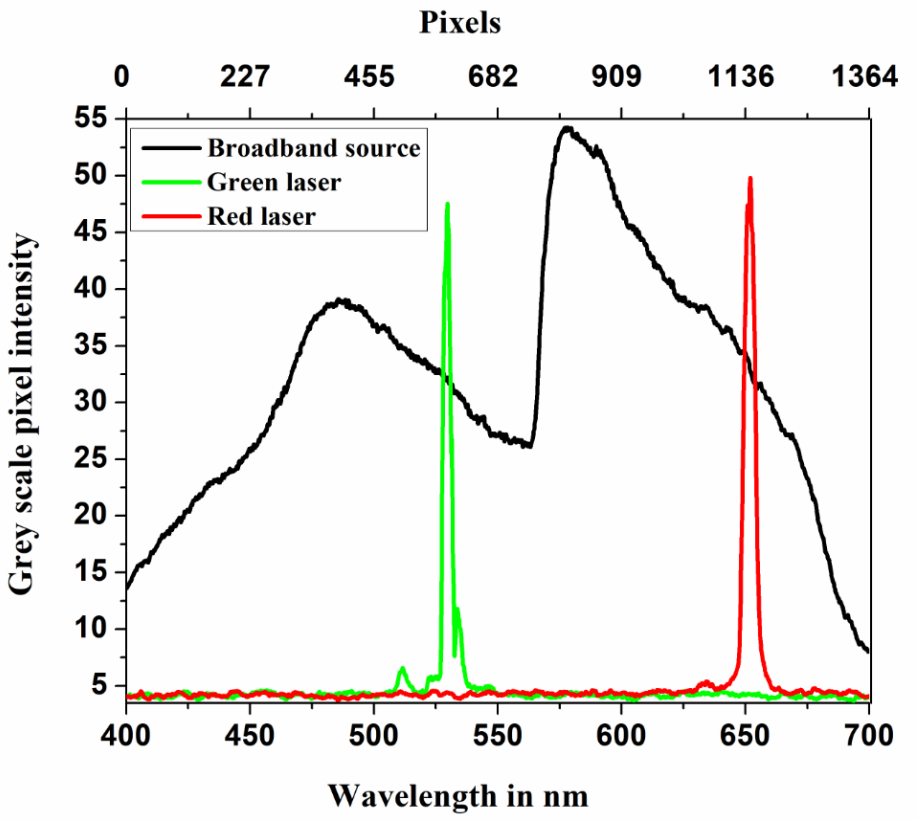

Figure 3.4: Pixel to wavelength scale conversion using broadband source and two other laser sources for the designed smartphone-based pH sensor.

be 1272 pixels and 717 pixels, respectively. The difference in pixel number of the two laser sources (555) has been correalated with the wavelength diffrence (122.5 nm). Therefore, 1 pixel shift is found to be (122.5/555) i.e. 0.22 nm. Upon converting the pixel to the wavelength scale, the spectral resolution of the developed sensor is obtained as 0.22 nm/pixel, which implies for every shift of pixel position, the wavelength will be shifted by 0.22 nm. The device has been calibrated with standard

pH samples ranging from 4 to 10 in an incremental step value of 1. An extended pH range has been considered in the present study to cover a broad soil pH range. The spectrum image of each dye treated sample has been recorded for ten consecutive times without removing it from the set-up to determine the transmittance. Upon recording the images for one sample, its average intensity value has been estimated and then convert it into the corresponding spectrum using Image-J App.

3.2.6 Spectrometric based pH sensing using smartphone

The characteristic spectra of standard dye treated pH samples have been analyzed to study the optical response of the designed smartphone-based sensor. Figure 3.5(a) shows the characteristic plot of the transmittance values recorded by our designed sensor. The captured spectrum images of each dye treated sample are shown as an inset in figure 3.5 (a). At 605 nm, the universal indicator dye shows peak transmittance conditions, with value decreasing with the increment of the samples' pH value. Although a spectral shift primarily in the wavelength range 500-550 nm has been occurred due to the change in the sample colour, but the spectral shift is not found to be correlating with the variation of pH values. However, a drop in the transmission intensity has been observed in the wavelength range 580-680 nm. This drop in intensity is due to the change in the colors of the pH samples from light pink to dark blue as shown in figure 3.1 , where the dark coloured samples with pH values absorbs more light and subsequently transmitting less light from the sample. The peak intensity variation with the pH values has been observed to be prominent at the wavelength 605 nm. Therefore, the wavelength 605 nm is considered as the peak wavelength condition where the transmission intensity is decreasing with the increase in pH values for sensing of the pH level in soil medium. The same samples' transmission plots have been recorded using a standard spectrophotometer (UV 2450, SHIMADZU). Figure 3.5(b) shows the characteristic plots of the same samples measured by the standard spectrophotometer. The detector used in the proposed smartphone based spectrometer is CMOS camera of the smartphone which is different from the detector used in standard UV-Visible spectrometer.i.e. a photomultiplier tube. Owing to the variation of detector characteristic in both the sensing setup, the spectral response of the universal dye treated pH sample has been found to be different from the standard UV-visible spectrometer. Also the application that has been used for processing the data in the smartphone is different from the software that is used in the commercial grade spectrometer. Therefore, the spectra recorded by the smartphone spectrometer is not exactly same with the spectra obtained with standard spectrometer. However, a similar trend of spectrometric intensity variation with the change in the pH value has been noticed.

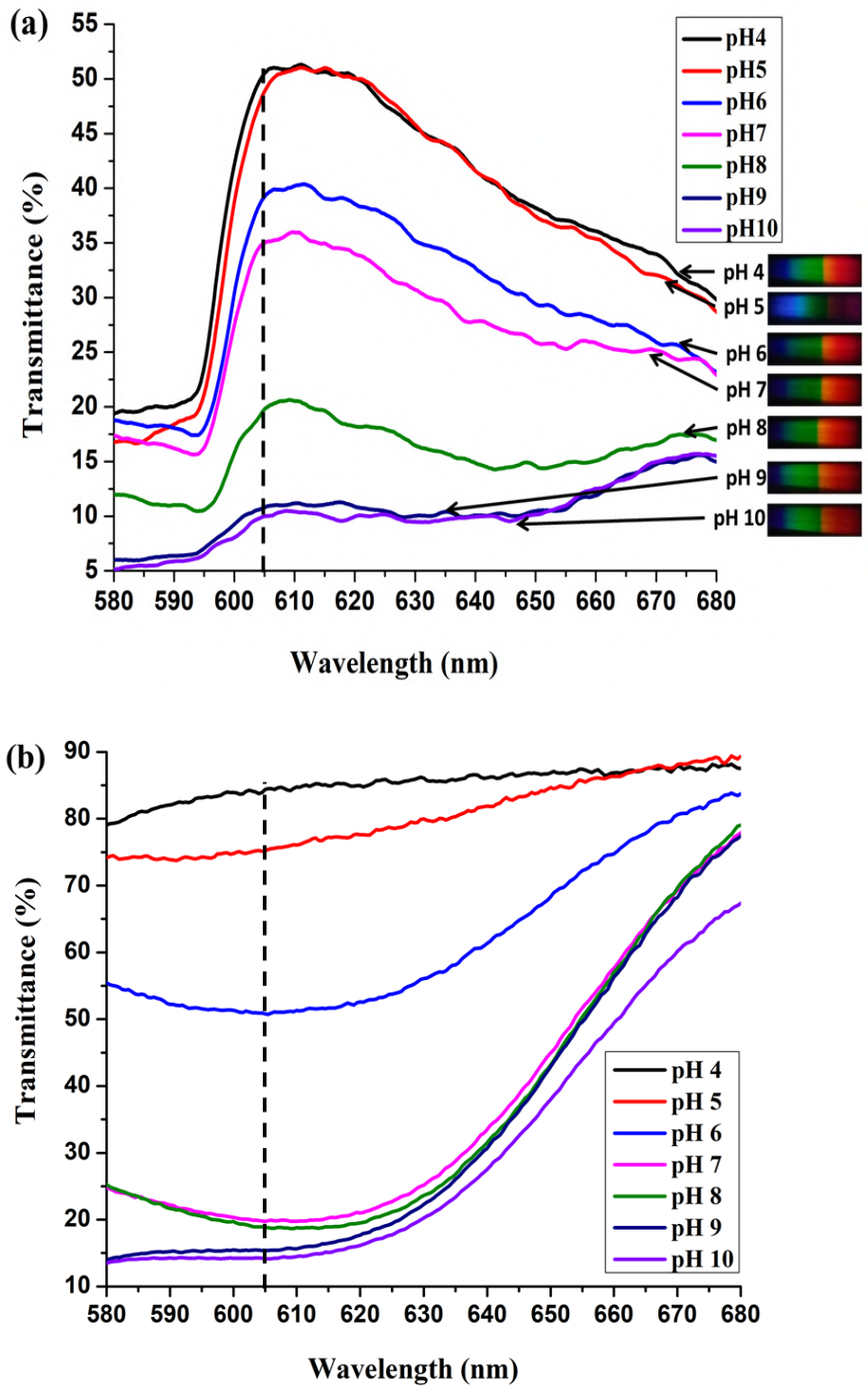

Figure 3.5: Characteristic transmission spectra of universal dye treated standard pH samples from 4 to 10 as obtained with (a) designed smartphone sensor (b) standard spectrophotometer.

In both the spectrum, the change in transmittance value at 605 nm is found to be correlating with the change in pH value. Using 'Origin software,' the regression analysis of the recorded data at 605 nm has been plotted, as shown in figure 3.6. From the regression analysis of the recorded data at 605 nm, a good linear fit has been

observed within the pH range 4 to 10 with a co-efficient of regression $R^2 = 0.96373$. Following calibration equation can be obtained from the regression analysis between pH value and the normalized transmittance value for our designed sensor:

$$pH = \frac{1.54581 - I}{0.12923} \tag{3.1}$$

where, I is the normalized transmittance value with respect to the broadband source at 605 nm as captured by the designed sensor. By plotting the % transmittance value, the pH value of an unknown sample can be estimated from equation 3.1. As shown in figure 3.5(a), at 605 nm peak wavelength, the designed sensor can discriminate the sensor response value well in the pH range 4 to 10. However, the sensitivity of the sensor is observed to be low in the low pH range between 4 and 5 and in the high range between 9 and 10 pH values of the medium. The sensitivity of the designed sensor is observed to be linear in the pH range 5 to 9 of the sample.

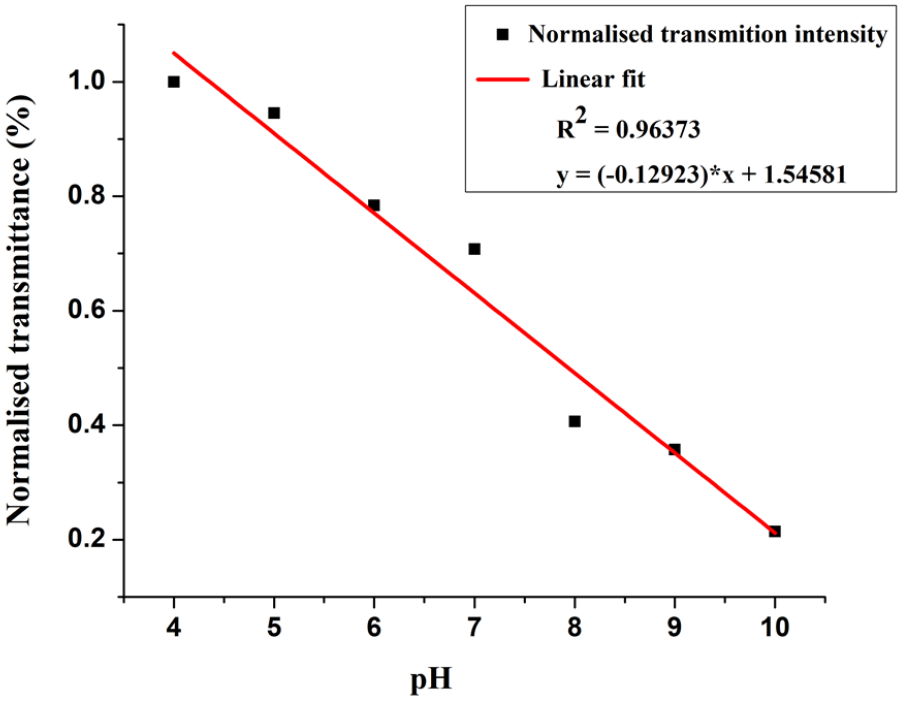

Figure 3.6: Characteristic normalized transmittance plot for standard pH samples from 4 to 10 obtained with the designed smartphone sensor.

3.2.7 Evaluation of different sensoristic parameters of the designed smartphone based photometric sensor

Important sensoristic parameters of the designed sensor have been evaluated and discussed as follows: **Sensitivity** of a sensor is defined as the change in output for a unit change in the input [28]. It represents the slope of the calibration curve. From the characteristic sensor response curve for dye treated pH samples ranging from pH 4

to 10, the sensitivity for the designed sensing tool is estimated to be 0.129 per pH unit. **Limit of detection (LoD)** is another important figure of merit of any sensor. It is the lowest concentration of an analyte likely to be reliably detected from the analyte having zero concentration [29]. As per the guidelines of the International Conference on Harmonization (ICH) [30], the LoD of a sensing system can be estimated from the following equation:

$$LoD = \frac{3.3\sigma}{S} \tag{3.2}$$

where, σ is the standard deviation of the y-intercept of the regression line, and S is the slope of the calibrated data. By putting the values of σ and S in equation 3.2, the theoretical value of LoD of the designed sensor is estimated to be 1.7 pH. However, the practical value of LoD for the designed tool is found to be 4 pH units. The performance of the designed sensor has further been evaluated by estimating its **accuracy** and **precision** value. To determine these parameters, we considered three standard pH samples with pH values 4, 7, and 10 so that it covers the low, medium, and high pH value within the calibration range. The pH values of these samples were initially measured with the standard pH meter before we estimate the values with the designed sensor. Each sample has been measured rapidly for five consecutive times, and the mean pH value and their respective standard deviation (SD) have been estimated. The accuracy is expressed as % bias from the calculated mean pH value as

$$\%bias = \frac{Known\ pH\ value - Mean\ pH\ value}{Known\ pH\ value} \times 100 \tag{3.3}$$

The precision is determined in terms of % residual standard deviations (% RSD) and is given as:

$$\%RSD = \frac{SD}{Mean} \times 100 \tag{3.4}$$

Table 3.1 shows the mean bias of accuracy of pH values and the mean RSD in precision for the considered samples. The mean bias accuracy is found to be 0.73%, while the mean RSD is 1.86%. The lower value of % RSD suggests a high accuracy of the designed tool while measuring the pH value of the sample.

In the next step, the reproducibility characteristic of the proposed sensor has been studied. A dye treated medium with a pH value of 5 has been considered as the test sample. The spectrum images of the sample were captured seven times by inserting the sample consecutively in the optical set-up. Figure 3.7 shows the characteristic transmittance plots recorded by the designed smartphone sensor. The transmittance plots indicate that there is no significant variation in the transmission characteristic of the sample. This, again, suggests a good degree of reproducibility of the designed

Table 3.1: Accuracy and precision data for pH value of buffer samples (n=3).

pH value buffer samples	**Mean**	**Standard deviation**	**Accuracy (% Bias)**	**Precision (% R.S.D)**
4	4.05	0.011	1.25	0.27048
7	7.04	0.015	0.685	0.20852
10	10.02	0.008	0.26	0.07979
			Mean % Bias = 0.73%	
				Mean %R.S.D = 1.86%

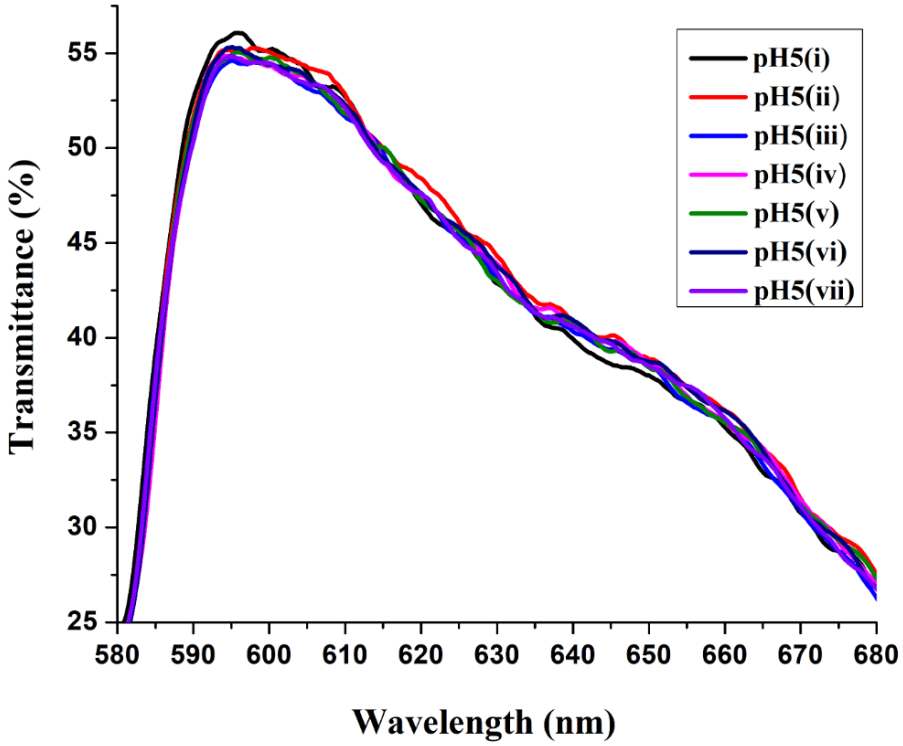

Figure 3.7: Transmission spectra of universal dye treated standard sample of pH 5 obtained with the designed smartphone sensor for seven consecutive measurements.

sensor.

3.2.8 Sensor performance for different field collected samples

To demonstrate the usability of the designed tool to measure the pH value of field-collected samples, six soil samples acquired from different farmlands, as described in section 3.2.3, have been prepared in the laboratory. Figure 3.8(a) shows the characteristic transmission spectra of the soil samples captured by the designed sensor. The sample's peak transmission responses at 605 nm are observed to be increasing with

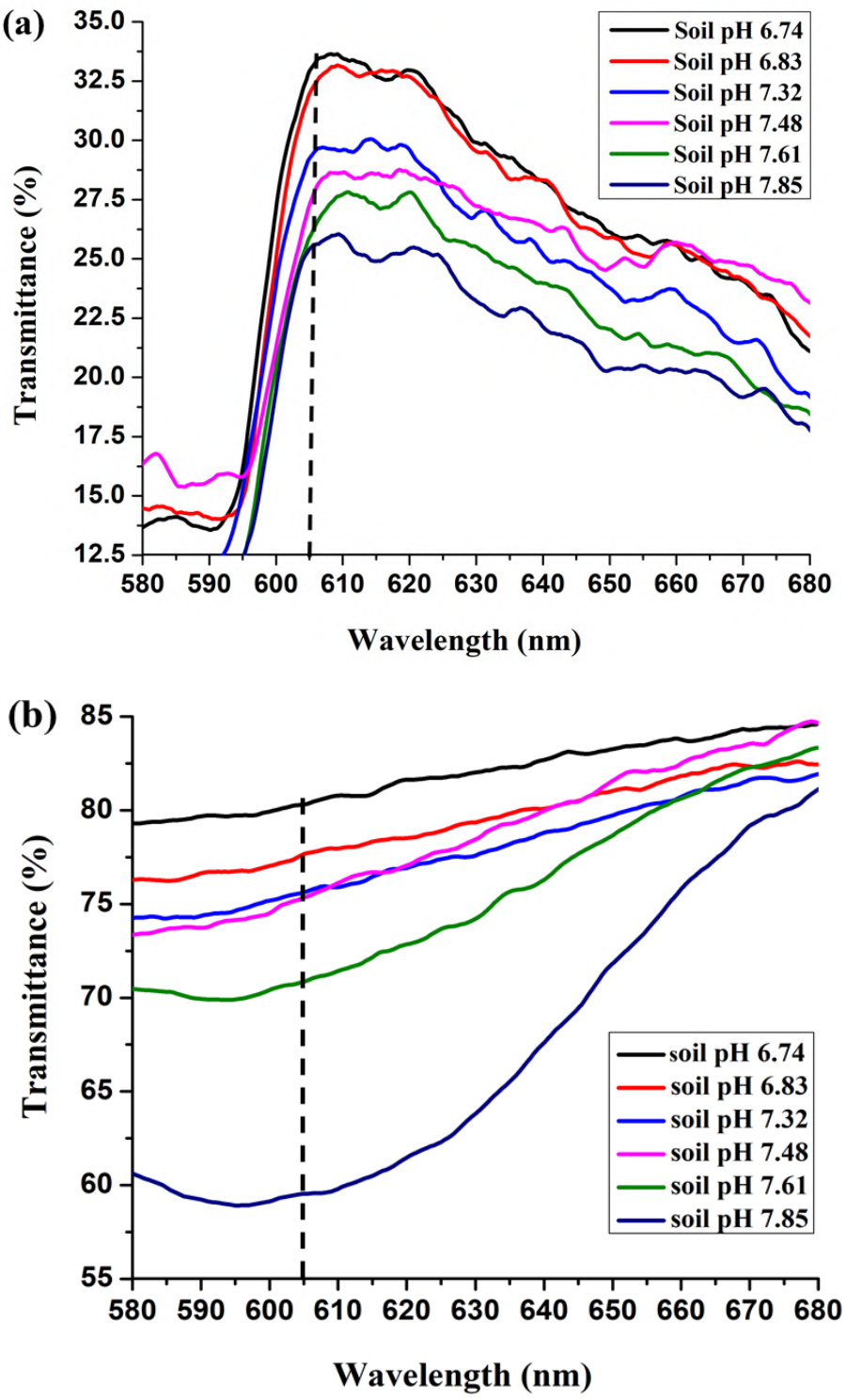

Figure 3.8: Characteristic transmittance plot of universal dye treated six field-collected soil samples obtained with (a) designed smartphone sensor (b) standard spectrophotometer.

the decrement of its pH value. Figure 3.8(b) shows the corresponding transmission plots of the same samples recorded by the standard spectrophotometer (UV 2450, SHIMADZU). The spectral data yield from both the tools can be easily correlated.

The designed sensor yields a distinguishable response for the soil samples even if the sample pH values are separated by 0.09 pH units. However, beyond this, the sensor is unable to discriminate the response. This indicates that the resolution of the proposed tool with the considered pH indicator dye is 0.09 pH unit in the pH range of 5 to 9.

Table 3.2 represents the pH value measurements by both the commercial pH meter and the smartphone sensor. The maximum variation in pH value measured by our designed sensor was found to be less than ± 5% than that of its commercial counterpart, which again suggests a good degree of reliability of the proposed tool.

Table 3.2: Measured pH value of field-collected soil samples by laboratory pH meter and smartphone optical sensor.

Soil samples	**pH value recorded by standard pH meter**	**pH value recorded by the smartphone platform pH sensor**
Sample 1	7.48	7.50
Sample 2	7.61	7.65
Sample 3	7.85	7.88
Sample 4	6.74	6.75
Sample 5	7.32	7.33
Sample 6	6.83	6.85

3.3 Extending the applicability of the designed smartphone-based spectrometer for the estimation of arsenic (As) and lead (Pb) ion concentrations in soil

In the present work the working of a compact smartphone-based LSPR sensing platform for quantitative detection of As(III) and Pb(II) in soil medium through modulating the LSPR band of gold nanoparticles (AuNPs) has been demonstrated. AuNPs functionalized with glucose (AuNPs/Glu) are found to be aggregated upon treatment with As(III) and Pb(II), which resulted the shifting of the LSPR band in the visible region due to the non-covalent interaction between the metal ions and AuNPs/Glu. The LSPR signal intensities of the AuNPs/Glu samples due to the presence of As(III) and Pb(II) in the samples have been recorded by the rear camera of smartphone. The concentration of As(III) and Pb(II) is quantitatively determined by measuring the signal intensities at peak absorption wavelength by the designed smartphone sensor.

The detection and analysis of the analytes is performed by using a custom designed android application- “Soil Quality Monitoring” (SoQM) to convert the designed sensor into a truly standalone tool. The results obtained with field-collected soil samples have been compared with standard laboratory grade tool. The following subsections provide more information on the methodologies used for detection of the mentioned metal ions.

3.3.1 Materials and methods

3.3.2 Chemicals and reagents

All the chemicals used in the present study are of analytical grade and have been used as received without further purification. Glucose, trisodium citrate, and chloroauric acid $AuHCl_4$ were procured from Sigma-Aldrich Inc. 1000 ppm of standard stock samples of both Arsenic and Lead were procured from Sigma-Aldrich Inc. Various working standard solutions of As(III) and Pb(II) were prepared by serially diluting the standard stock solution. For maintaining the pH level of the sample solution, 0.1 M solutions of both hydrogen chloride (HCl) and sodium hydroxide NaOH (ACS reagent, 97%, Sigma-Aldrich) have been prepared in the laboratory and mixed with the solutions in proportionate amount.

3.3.3 Instrumentation

The size and shape of the synthesized AuNP/Glu sample were first investigated by acquiring the images with a transmission electron microscope (TECNAI G2 20 S-TWIN, FEI Company). The LSPR absorption signal intensities from the AuNP/Glu sample were recorded with a standard UV−visible spectrometer (Shimadzu/ UV-1700). The pH levels of the prepared samples was maintained using a laboratory standard pH meter (Cyber Scan pH 700). The metal ion content in the field collected samples were measured by Atomic Absorption Spectrometer (Thermo Scientific, UK Model: AAS-ICE 3500 AAS) and Inductively Coupled Plasma optical Emission Spectrophotometer (Perkin Elmer/ Optima 2100DV). The deionized (DI) water used for preparation of the samples was acquired from a Milli-Q water filtering system.

3.3.4 Synthesis of the functionalized gold nanoparticles

AuNP/Glu has been synthesized in the laboratory by treating trisodium citrate as the reducing agent during the reduction process of $AuHCl_4$, while glucose was served as a stabilising agent [31]. In a conical flask, 40 mL of aqueous solution of $HAuCl_4$ (195 mM) was heated to 100℃ and then the solution was immediately mixed with 540 µL trisodium citrate (0.1 M). The solution mixture turned into pink color indicating

the formation of AuNPs in the absence of stabilizing agent. The solution mixture was then heated at 100°C for 2 hours and then centrifuged for 20 min at 7000 RPM to remove the excess trisodium citrate from the AuNP solution. In the next step, 0.5 mL of glucose solution (0.05 mM) was added into 40 mL of the synthesized AuNPs, and after that sonication was carried out for ligand exchange reaction. To remove any remaining ligands from the solution, the nanoparticles colloidal suspension was again centrifuged at 7000 rpm for 20 min. The prepared nanoparticles were stored at 4°C for further use.

3.3.5 Sample preparation

Standard solutions of As(III) and Pb(II) of varying concentrations in the range 5-50 ppm have been synthesized from the stock solution by diluting serially with distilled water. 1 mL of each standard solution was added to 4 mL of AuNP/Glu solution and adjusted the pH value at 7.0 by adding 0.1 M solutions of HCl or NaOH. All the prepared standard samples were then kept at room temperature for 10 min to observe the chemical reaction and the color shift of the nanoparticles. The color of the nanoparticle solution gradually changes from pink to purple and bluish grey on addition of As(III) and Pb(II), respectively, indicating the agglomeration of the AuNPs in the presence of the target ions.

3.3.6 Design and calibration of the sensing setup

The experimental setup as illustrated in section 3.2.4 has been modified for the present sensing studies. The DVD grating was replaced with a laboratory grade transmission grating for better sensitivity. Also, the sensor has been calibrated with LEDs instead of laser sources. The LEDs can be powered by smartphone's internal battery by connecting with USB-OTG cable which reduces the requirement of external power supply and also minimises the cost of the device. The schematic diagram and photoimage of the modified setup are shown in figure 3.9 (a) and 3.9 (b), respectively. To convert the pixel position to wavelength information first the dispersed spectrums of the three LEDs with peak wavelength 470 nm, 525 nm and 636 nm have been captured and from the captured images the grey scale intensity values have been extracted by using the developed android application "SoQM". The dispersed spectra of the three LEDs are shown in figure 3.10(a). The pixel positions and the respective peak wavelengths of the LEDs have been fitted from these spectra data and a linear equation has been obtained as shown in figure 3.10(b). The developed sensor has a spectral resolution of 0.25 nm/pixel when converted to wavelength scale, indicating that for every change in pixel position, the wavelength will shift by 0.25 nm.

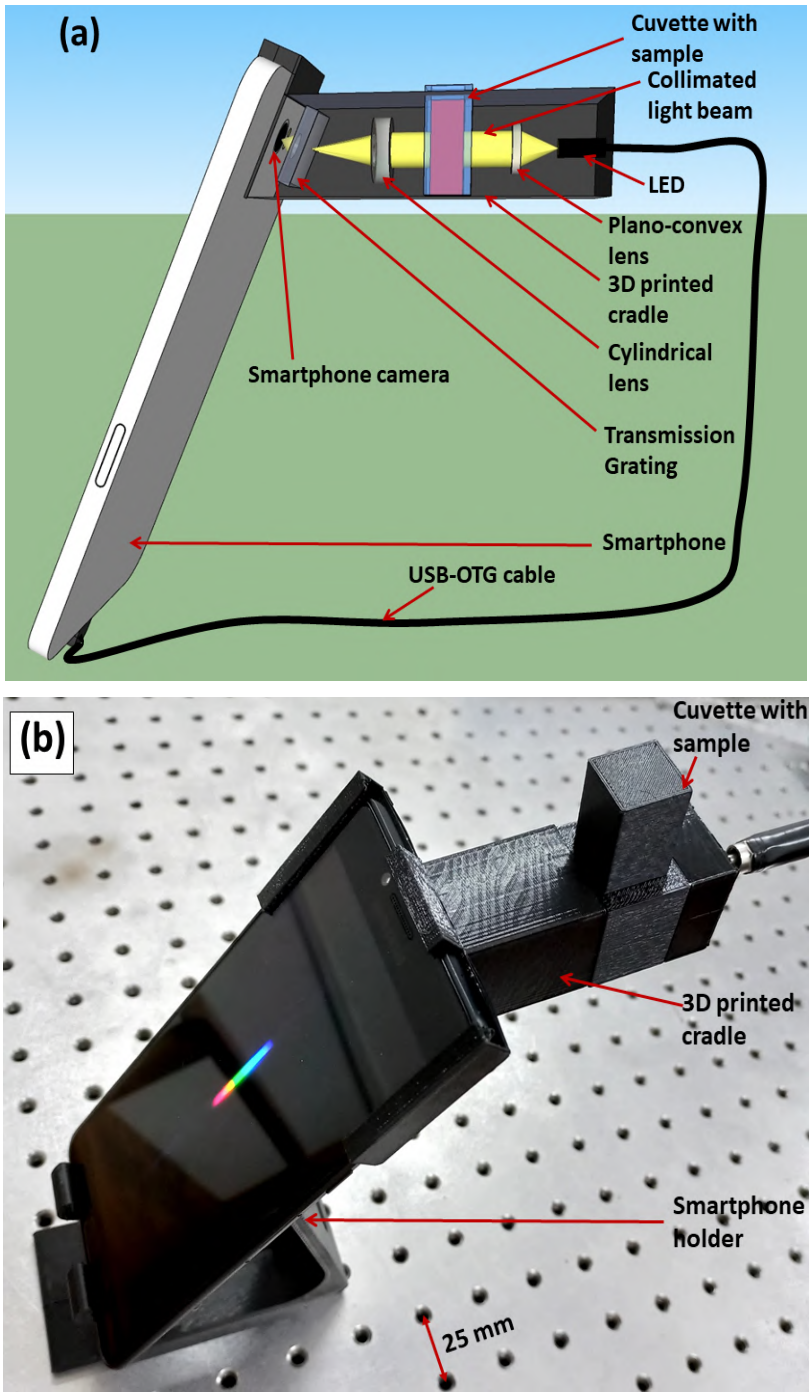

Figure 3.9: (a) Schematic diagram of the designed smartphone sensor (b) Photoimage of the designed smartphone sensor.

3.3.7 Development of the android application

A custom designed android application, "Soil Quality Monitoring" (SoQM) has been developed to analyse the recorded data within the phone itself. The application has been designed using "MIT App Inventor 2" a cloud-based application developer platform that allows users to design and create applications based on individual needs [32]. Several important features are needed to be incorporated in the algorithm of the

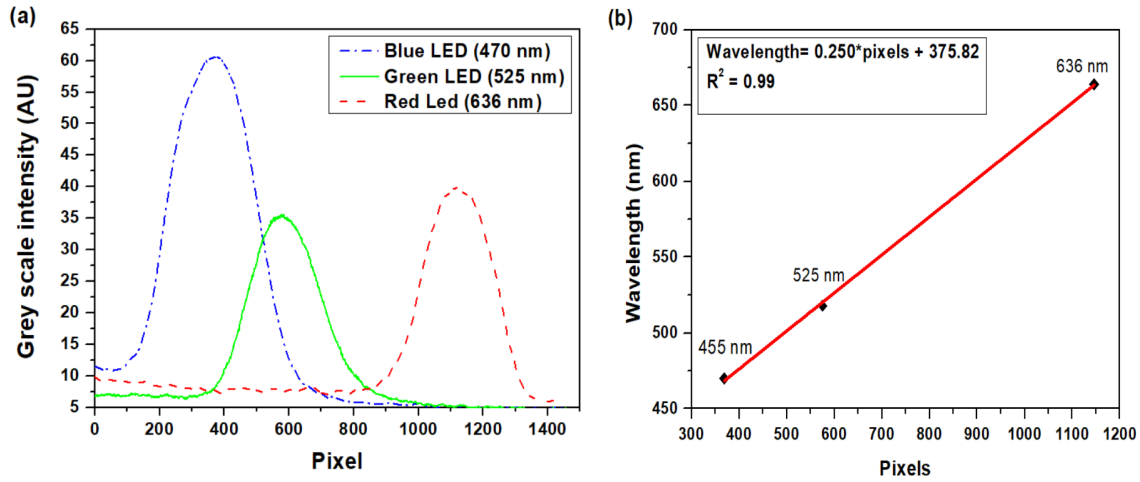

Figure 3.10: (a) Intensity vs pixel plot of three LEDs obtained by the designed sensor and (b) Pixel to wavelength calibration of developed sensor.

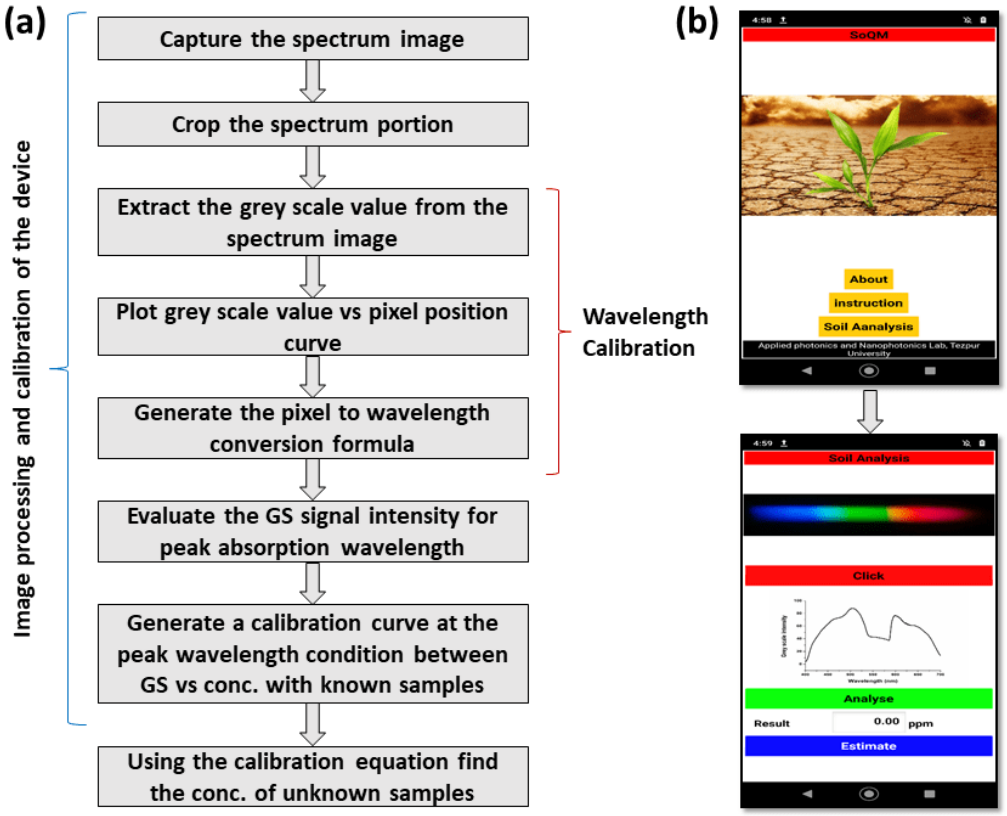

Figure 3.11: (a) Workflow and (b) screen shot images of the custom developed android application "SoQM".

designed application in order to transform the experimental data to a readable format. Figure 3.11(a) and 3.11(b) shows the process flow and some screen shot images of the developed android application, respectively. The designed sensor is required to be well calibrated to estimate the parameter of interest. The calibration part is critical to ensure the accuracy of the spectrum that is extracted from the spectrum image

recorded by any smartphone camera. For different variants of smartphone the camera specifications are diffrenet. In that case, the calibration process might be done prior to the measurement of the samples but it can be done within the application itself. In the custom designed application, the calibration feature has been included and given with step by step instructions. To do this user needs to click on the "soil analysis" button on the home screen of the SoQM. Upon hitting this two options- "capture" or "load" will pop up on the screen. User can capture the spectrum image directly by clicking the "capture" button or the earlier captured images can be loaded by clicking the "load" button. After this step, the spectrum portion of the image needs to be cropped in order to extract the grey scale value from the recorded image spectrum. By using image processing algorithm incorporated in the designed application, the grey scale intensity values of the captured images can be scanned over a wavelength range of 400-700 nm. The wavelength length range on X-axis and the grey scale values of the images on Y-axis are plotted with the help of the application. The grey scale intensity values of known concentration of As(III) and Pb(II) samples at their respective peak wavelength condition are recorded and from the recoded data a calibration equation is obtained. The generated calibration equation is embedded in the application algorithm so that the concentration of an unknown sample can be obtained by clicking the "analyse" button in the application. Finally, the analysed data may be shared online via the smartphone's internet functionality or it can be stored on the phone as a text file for future record.

3.3.8 Characterization of the nanoparticles

The morphology and particle size of the synthesized AuNP/Glu were examined by transmission electron microscopy (TEM). The change in particle size of AuNPs/Glu without and in presence of the analyte samples were confirmed by TEM imaging. The TEM images for the synthesized AuNP/Glu were clearly indicate that the AuNPs were spherical in shape, monodisperse in nature, and well-dispersed in aqueous solution in the absence of metal ions (As(III) and Pb(II)). The TEM images of AuNPs/Glu with and without the addition of As(III) and Pb(II) metal ions are given in figure 3.12(a), 3.12(b) and 3.12(c), respectively. The mean diameter of dispersed AuNPs/Glu is observed to be around 12 nm and aggregated AuNPs/Glu in presence of As(III) and Pb(II) were found to be 25 nm and 32 nm, respectively.

3.3.9 Mechanism for detection of As(III) and Pb(II) utilising AuNPs and Glucose as chemical sensor

The colloidal AuNP/Glu solution shows colorimetric variation in presence of As(III) and Pb(II) in the medium. As shown in figure 3.13(a) the AuNPs/Glu exhibits a

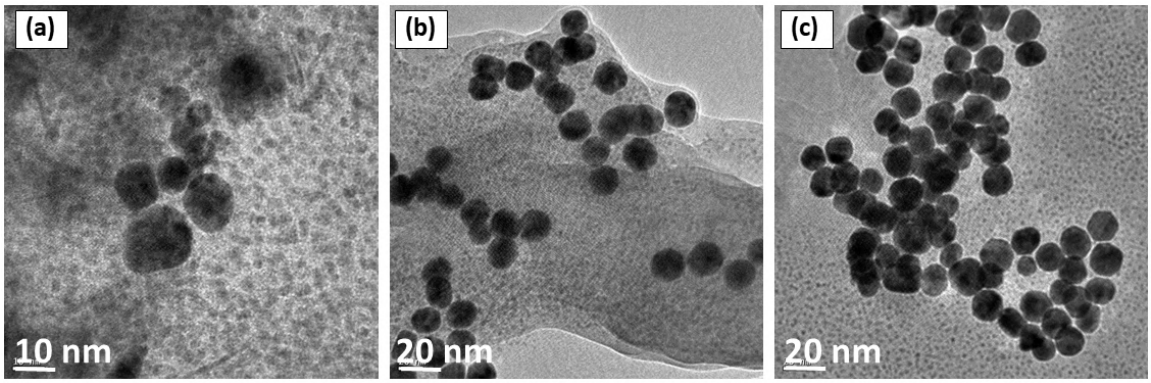

Figure 3.12: TEM image of (a) synthesized AuNPs/Glu, (b) aggregate AuNPs/Glu with As(III), (c) aggregate AuNPs/Glu with Pb(II).

mono-dispersion in the aqueous solution (pink colour) attributed to the presence of glucose molecules on the surface of NPs containing oxygen and hydroxyl groups, that prevents self-agglomeration of AuNPs. However, the colour of the NPs solution changes from pink to purple (figure 3.13(b)) and from pink to bluish grey (figure 3.13(c)) on the addition of As(III) and Pb(II) to the sample, respectively. The UV-Vis spectrum of AuNPs/Glu showed a distinct LSPR absorption band at around 520 nm shown in figure 3.13(d). The occurrence of the LSPR absorption peak at 520 nm suggests the formation of AuNPs of 10–50 nm size range [33, 34]. Upon addition of As(III) and Pb(II) to the AuNPs/Glu, the aggregation of nanoparticles occurred resulting the increase in size of the nanoparticles as confirmed by the TEM images shown in figure 3.13(b) and 3.13(c), respectively. The mean diameter of dispersed AuNPs/Glu is observed to be around 12 nm and aggregated AuNPs/Glu in presence of As(III) and Pb(II) were found to be 25 nm and 32 nm, respectively. The increase in the hydrodynamic diameter is attributed to analyte aggregation and a decrease in the electrostatic interaction between the analyte and AuNPs/Glu due to the chemical adsorption process [35]. Because of the aggregation of the NPs, a red shift has been observed for As(III) from 520 nm to 650 nm while for Pb(II) this has been shifted to 680 nm, respectively. The aggregation of NPs leads to the decrease in the inter-particle distance among the particles that causes an enhancement of the localized electric field, which is the primary reason for red shift in the LSPR band due to the presence of As(III) and Pb(II) in the sensing medium. The optical properties of gold nanoparticles change when particles aggregate and the conduction electrons near each particle surface become delocalized and are shared amongst neighboring particles. When this occurs, the surface plasmon resonance shifts to lower energies, causing the absorption and scattering peaks to red-shift to longer wavelengths [36–38]. Therefore, on addition of As(III) to the AuNPs/Glu, aggregation of the NPs, a red shift has been observed from 520 nm to 650 nm while for Pb(II) this has been shifted to 680 nm, as shown in figure 3.14(a) and 3.14(b), respectively. The sensing mechanism is based

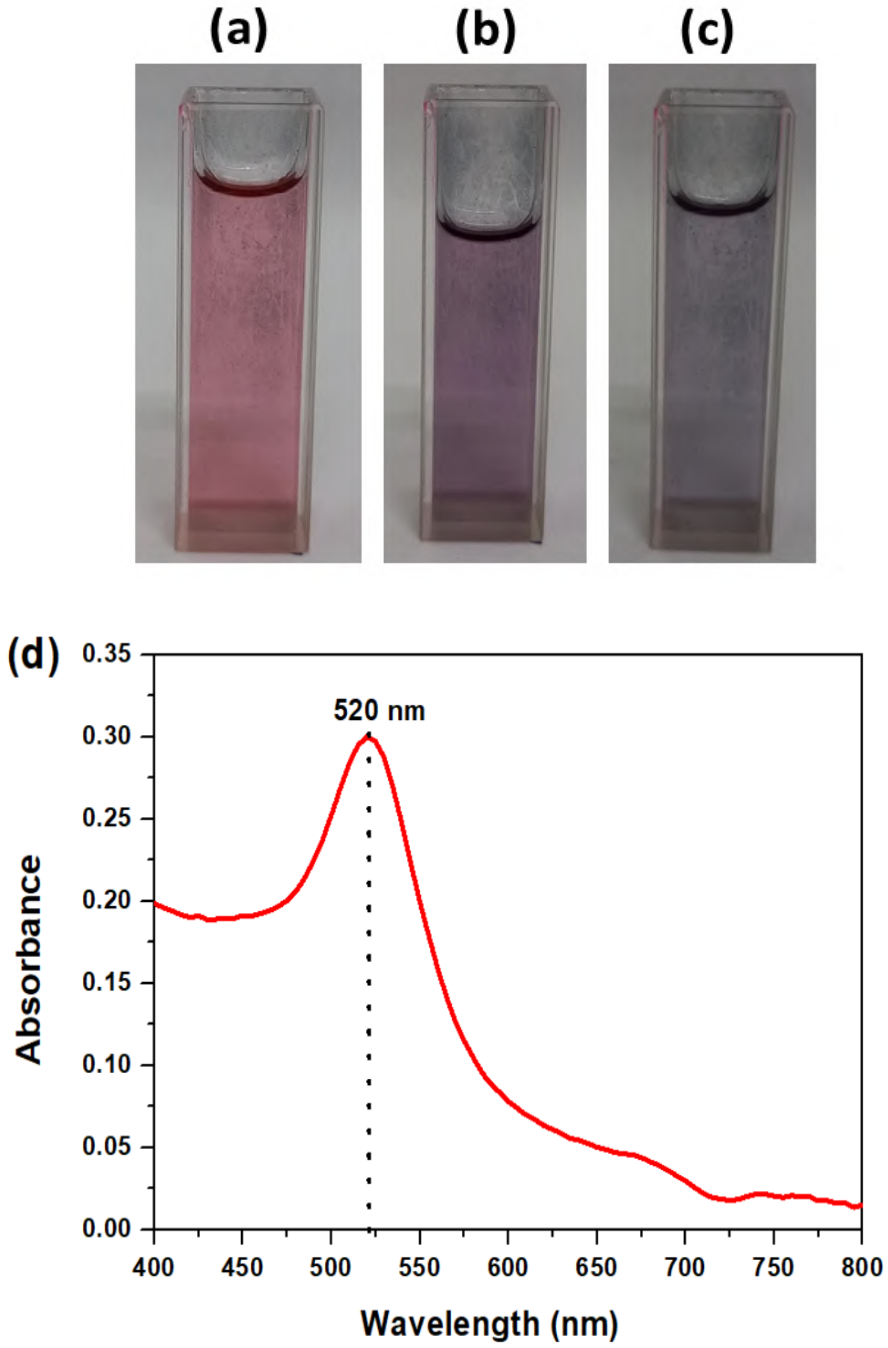

Figure 3.13: Photo images of cuvette containg (a) synthesized AuNPs/Glu, (b) AuNPs/Glu mixed with As(III), and (c) AuNPs/Glu mixed with Pb(II) and (d) UV-Vis spectrum of synthesized AuNPs/Glu.

on the interaction of glucose at the surface of the AuNPs. The sensing mechanism for the detection of As(III) and Pb(II) ion using AuNP/Glu has been illustrated in figure 3.15. The reaction between the analyte and AuNPs/Glu is completed in three steps as shown the figure 3.16. Step-I in figure 3.16 describes the preparation of AuNPs utilising the standard process and trisodium citrate as a reducing agent [31]. The interaction of the hydrogen bond with the carboxylate group of trisodium

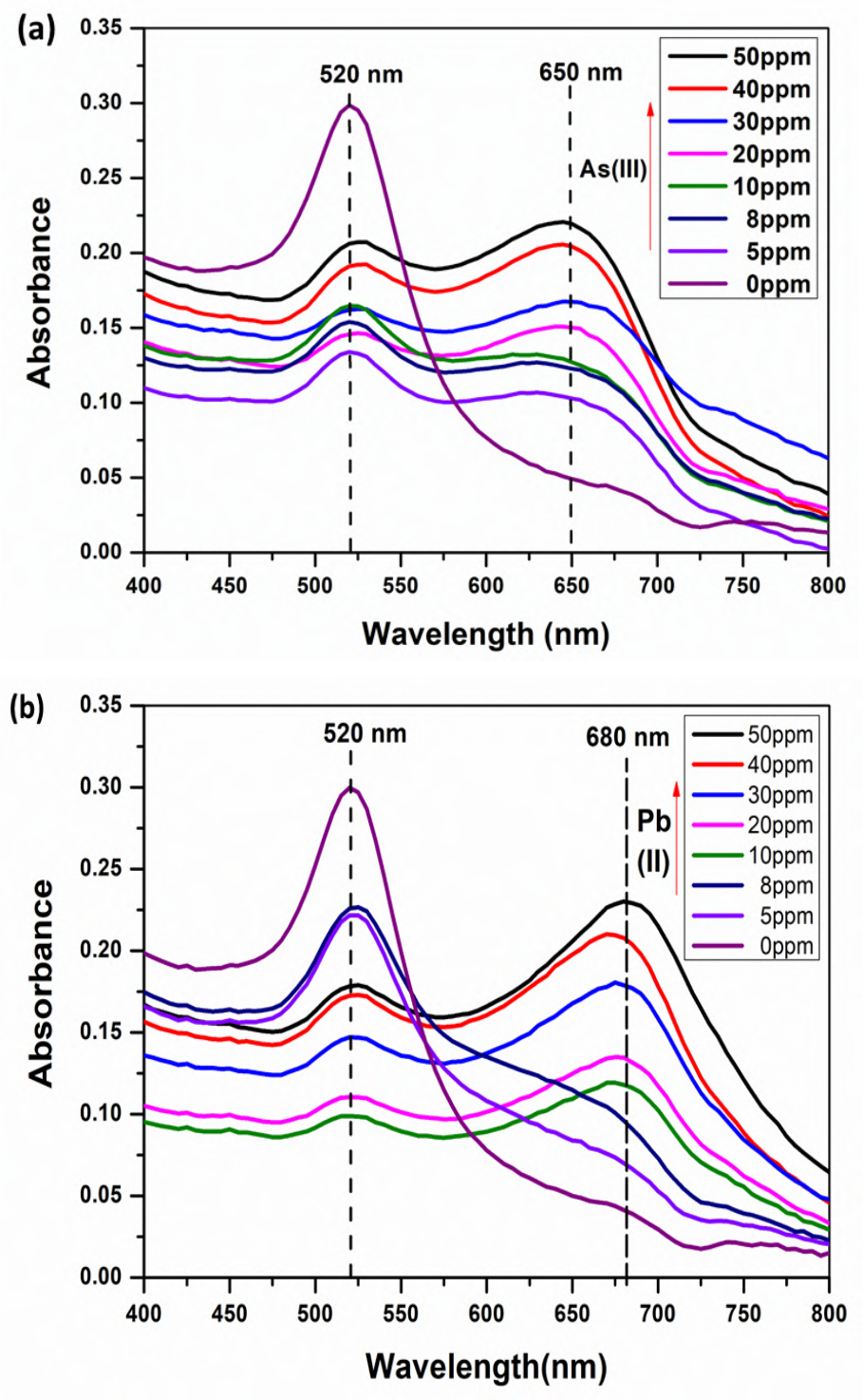

Figure 3.14: UV-Vis spectra of synthesized AuNPs/Glu mixed with various concentrations of (a) As(III) and (b) Pb(II).

citrate resulted in a significant adsorption of the compound onto the colloidal AuNPs surface.

In Step-II, glucose was added as a functionalizing agent to the citrate-stabilized AuNPs in order to modify their surface. The OH groups present in glucose molecules have a high affinity for As(III) and Pb(II) metal ions in aqueous media. The ex-

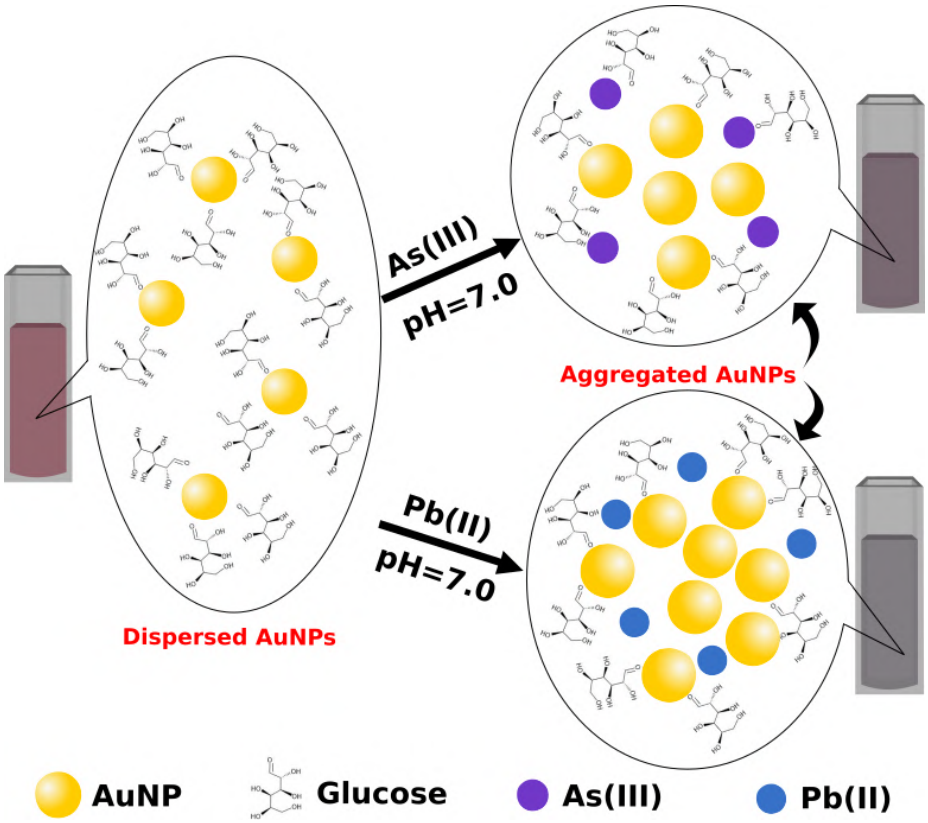

Figure 3.15: Plausible mechanism for the detection of As(III) and Pb(II) ion using AuNP/Glu.

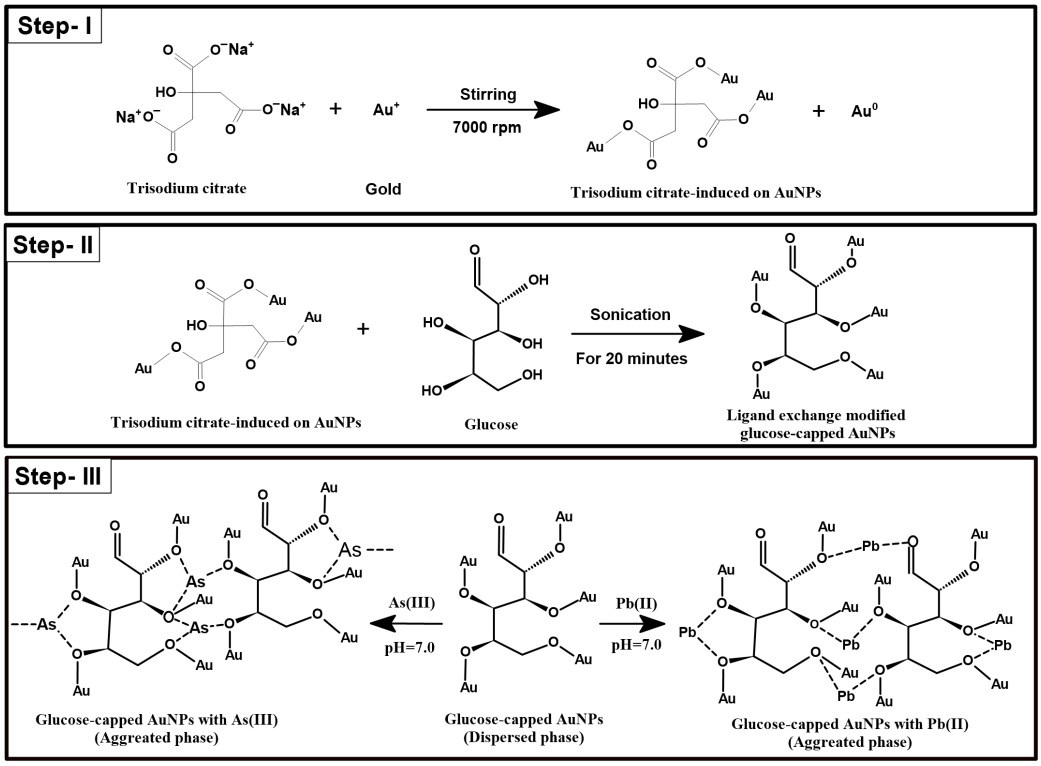

Figure 3.16: Probable reaction pathways in the determination of As(III) and Pb(II) using AuNPs/Glu.

cess ligands (the carboxylate group of citrate molecules) were immediately removed by sonicating the solution mixture of NPs for the ligand exchange reaction (LER) for 15 minutes. At that instant, the hydroxyl ion (-OH) of the glucose molecule interacts with the colloidal gold solution providing the AuNPs more stability than the citrate molecules. Furthermore, the glucose-stabilized AuNPs limit NPs' tendency to aggregate on their own or with other ionic substances. As a result, the interaction of the hydrogen bond in an aqueous solution causes the terminal portion of glucose on the surface of NPs to join with the Au-O bond to generate surface-modified AuNPs. On addition of As(III) and Pb(II), the colour of AuNPs/Glu sample changes. This colour change can be attributed by electrostatic and non-covalent interactions between As(III) and Pb(II) and AuNPs/Glu (Step-III). During the interaction with the AuNPs, glucose molecules form a new stabilising As-O bond by breaking the Au-O bond. Similarly, non-covalent interaction has been observed between the Pb(II) ion and the glucose-capped AuNPs. However, the AuNPs/Glu solution on addition of As(III) and Pb(II) exhibits a decrease in the LSPR peak at 520 nm while a broader band is appeared in the longer wavelength region, which suggests the binding of the analyte with glucose molecules. Upon treatment with As(III) a new absorption band centred at 650 nm has been appeared in the UV-vis spectra of AuNPs/Glu as shown in figure 3.14(a). The signal intensities of As(III) mixed AuNPs/Glu vary with the concentration of As(III) in the samples. Similarly, for AuNPs/Glu samples, on adding Pb(II) to the sample, a new absorption band centred at 680 nm appeared and the signal intensities of the samples at this peak wavelength condition increases with the concentration of Pb(II) in the mixture as shown in figure 3.14(b). These variations of the signal intensities with analyte's concentrations have been used for quantitative determination of As(III) and Pb(II) present in the samples.

3.3.10 Calibration of the designed smartphone sensing system for detection of As(III) and Pb(II)

The AuNP/Glu sample exhibits colorimetric change upon addition of As(III) and Pb(II) to the sample. At first the device has been calibrated with AuNP/Glu treated with standard As(III) samples for varying concentrations of As in the range 5-50 ppm. The characteristic absorption spectra of these samples has been recorded with the designed sensor and is shown in figure 3.17(a). Clearly, the LSPR peak of the AuNP/Glu at 520 nm is seen to be decreased while a new absorption peak appears at 650 nm on addition of As(III), which is in agreement with the standard UV-Vis spectral data discussed in section 3.3.9. Figure 3.17(a) shows that at the newly appeared absorption peak of wavelength 650 nm, the signal intensities of the As(III) treated AuNP/Glu samples increases with the concentration of the As(III) present

in the samples. The signal intensity variations at 650 nm vs the concentrations of As(III) in the range of 5-50 ppm has been plotted to perform quantitative analysis of As(III), and a linear fitted graph with a regression coefficient value $R^2 = 0.98$ has been obtained as shown in figure 3.17(b).

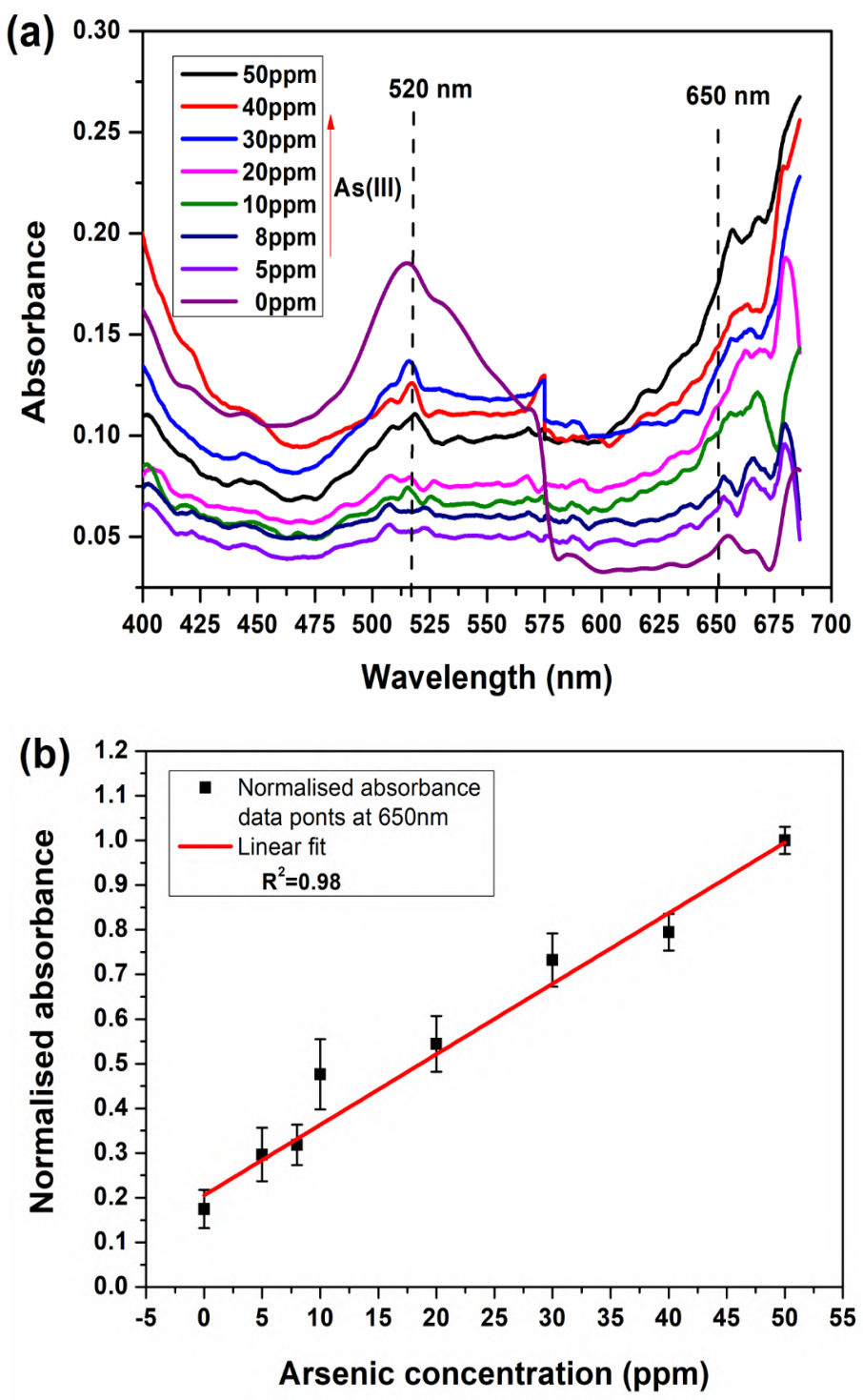

Figure 3.17: (a) Absorbance plot of AuNP/Glu samples mixed with As(III) in the concentration range 5-50 ppm (b) linear fitted plot at peak absorbance condition as recorded by the designed sensor.

The error bar in the graph represents the standard deviations for five consecutive measurements of each sample recorded by the designed smartphone sensor. From the linear fitted graph, a calibration equation has been obtained for detection of As(III) levels as given below:

$$Arsenic(III)conc. = \frac{Normalized\ Absorbance - 0.20536}{0.01579} \tag{3.5}$$

where, normalized intensity is the normalized sensor response recorded by the designed sensor.

For the quantitative estimation of Pb(II), the designed sensor has also been calibrated with standard Pb(II) samples in the concentration range 5-50 ppm mixed with AuNP/Glu solutions. Figure 3.18(a) shows the characteristic absorbance plot of the aggregated AuNP/Glu with Pb(II) samples as recorded by the smartphone sensor. Figure 3.18(a) it can be observed that the absorbance values at the peak wavelength 680 nm increases with Pb(II) in the samples, which is similar to the UV-Vis absorption spectra illustrated in figure 3.14(b). The changes in absorbance values at the peak wavelength condition 680 nm with the Pb(II) concentration in the range 5-50 ppm has been plotted to study the variation, and a linearly fitted curve has been obtained with regression coefficient of $R^2 = 0.99$ as given in figure 3.18(b). The error bars in the graph shows the sensor response's standard deviations for five successive measurements of each sample. From the calibration curve a calibration equation has been obtained to measure Pb(II) concentration of unknown sample:

$$Lead(II)conc. = \frac{Normalized\ Absorbance - 0.1414}{0.01757} \tag{3.6}$$

Using the equation 3.5 and 3.6, the developed smartphone sensing tool has been initially calibrated for detection and estimation of As(III) and Pb(II) concentration of unknown samples. The user can use the equations 3.5 and 3.6 to calculate the unknown concentration after measuring the absorbance value of a specific analyte.

3.3.11 Evaluation of sensoristic parameters of the designed sensor

Sensitivity and Limit of detection (LoD) are two important parameters of a sensor. Sensitivity represents the change in output for a unit change in the input [28]. The sensitivity of the designed sensor while measuring As(III) and Pb(II) is calculated from the slope of the calibration curves given in figure 3.17(b) and 3.18(b), respectively. For the proposed sensing platform, sensitivity of the sensor are found to be 0.01579 A.U./ppm and 0.01757 A.U./ppm, while monitoring the As(III) and Pb(II), respectively. According to the International Conference on Harmonization

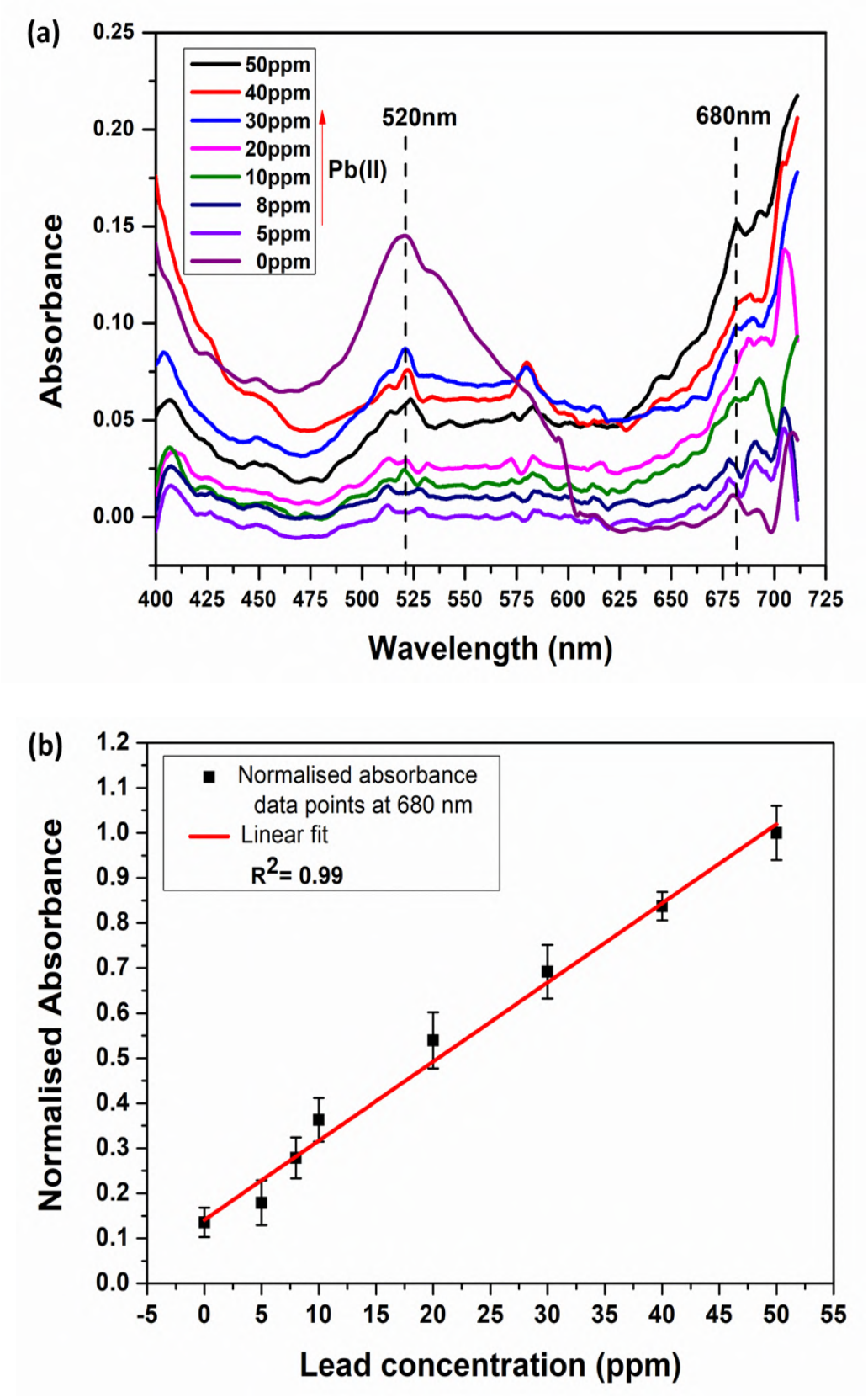

Figure 3.18: (a) Absorbance plot of AuNP/Glu samples mixed with Pb(II) in the concentration range 5-50 ppm (b) linear fitted plot at peak absorbance condition as recorded by the designed sensor.

(ICH) guidelines [29, 30], the LoD is calculated using the following equation:

$$LoD = \frac{3.3\sigma}{S} \tag{3.7}$$

where S is the slope of the calibration curve and is σ the standard deviation of the regression line's y-intercept. The LoDs are calculated to be 1.2 ppm and 1.5 ppm for As(III) and Pb(II), respectively.

3.3.12 Effect of interfering ions on the measurement of As(III) and Pb(II)

The interference of other ions on the measurement of the As(III) and Pb(II) is a crucial factor before considering the reliability of the present sensing scheme. AuNPs/Glu samples were mixed with several metal ions that might be present in soil samples, including K(I), Na(I), Mg(II), Ca(II), Mn(II), Co(II), Ni(II), Zn(II), Cu(II), Cd(II), Hg(II), Al(III), Fe(III), and Cr(IV) under optimal condition. 1 nM solution of each of the interfering elements that may possibly be present in soil medium has been added to AuNPs/Glu sample mixed with 5 ppm of standard As(III) and Pb(II) sample. The concentration of As(III) and Pb(II) sample in the presence of each interfering element has been measured by the smartphone-based sensor and the results have been compared with the data obtained using a laboratory grade inductive coupled plasma spectrometer and atomic absorption spectrophotometer. Figure 3.19(a) and 3.19(b) shows a bar graph comparison of the designed sensor's anti-interference performance against that of the standard tools for As(III) and Pb(II) detection, respectively. A tolerable low fluctuation of about 3% in the As(III) and Pb(II) measurement has been observed. These results yet again suggest that even in the presence of interfering components in the test sample, the proposed sensing system can be employed to reliably monitor the As(III) and Pb(II) concentration in soil medium.

3.3.13 Evaluation of sensor performance for field-collected sample

The performances of the developed sensing schemes have been evaluated for field-collected soil samples. Fifteen soil samples (S1—S15) have been acquired from different farmlands to investigate the As(III) and Pb(II) concentration in the soil samples with the designed sensor. Following the standard protocol reported elsewhere [39, 40], the soil samples have been prepared in the laboratory for extraction of As(III) and Pb(II) from the soil samples. In some of the soil samples, As(III) and Pb(II) have been spiked due to the presence of very low level concentrations of the target analyte in soil. Figure 3.20(a) and 3.20(b) illustrate the bar-graph comparison of the

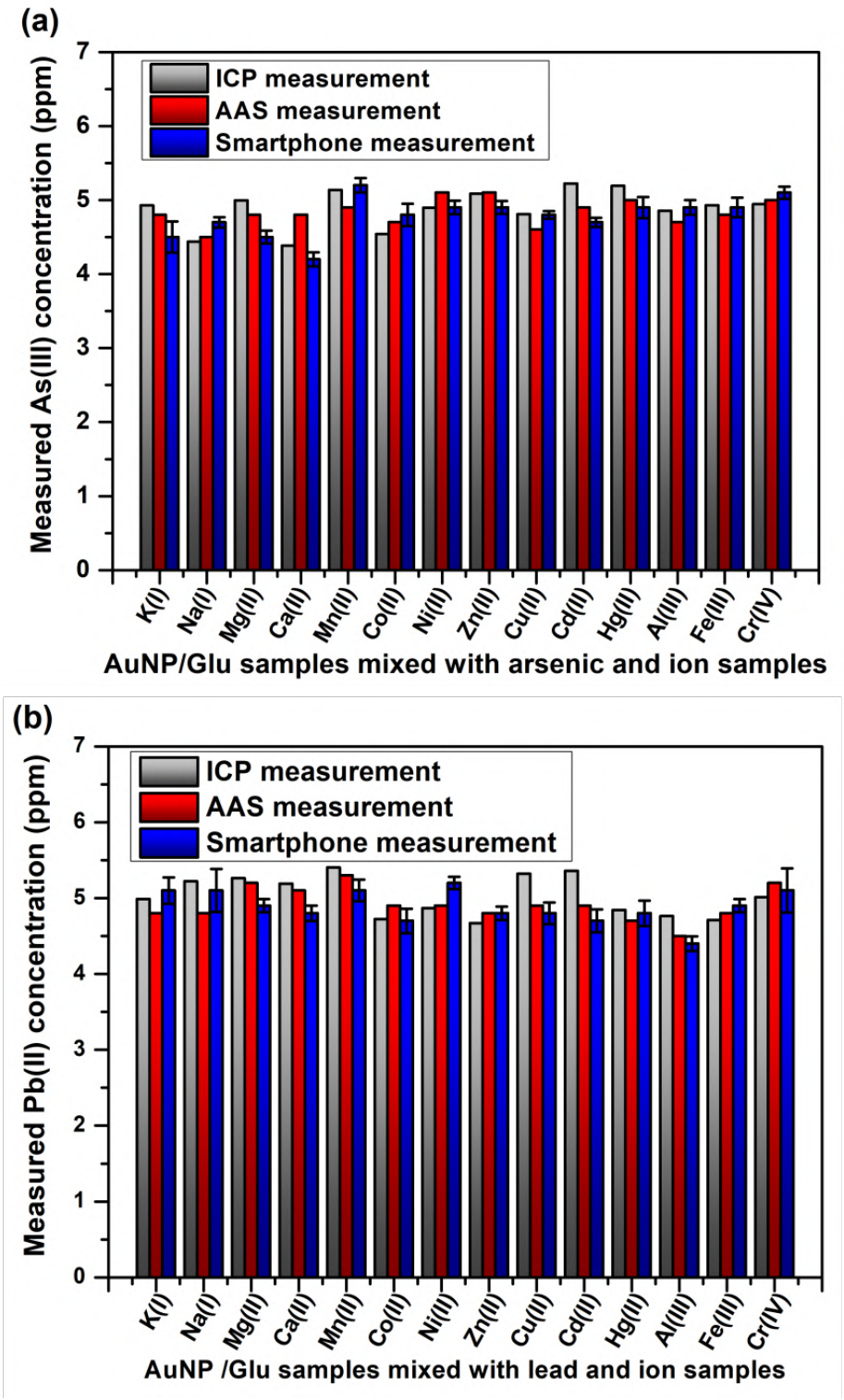

Figure 3.19: Comparative bar-graph illustration of measurements done by the standard inductive coupled plasma spectrometer, atomic absorption spectrophotometer, and designed smartphone-based sensor for AuNP/Glu samples mixed with considered interfering ions for the detection of (a) Arsenic(III) and (b) Lead(II).

smartphone sensing data, the standard atomic absorption spectrophotometer data and the inductive coupled plasma (Perkin Elmer/ Optima 2100DV) measurements

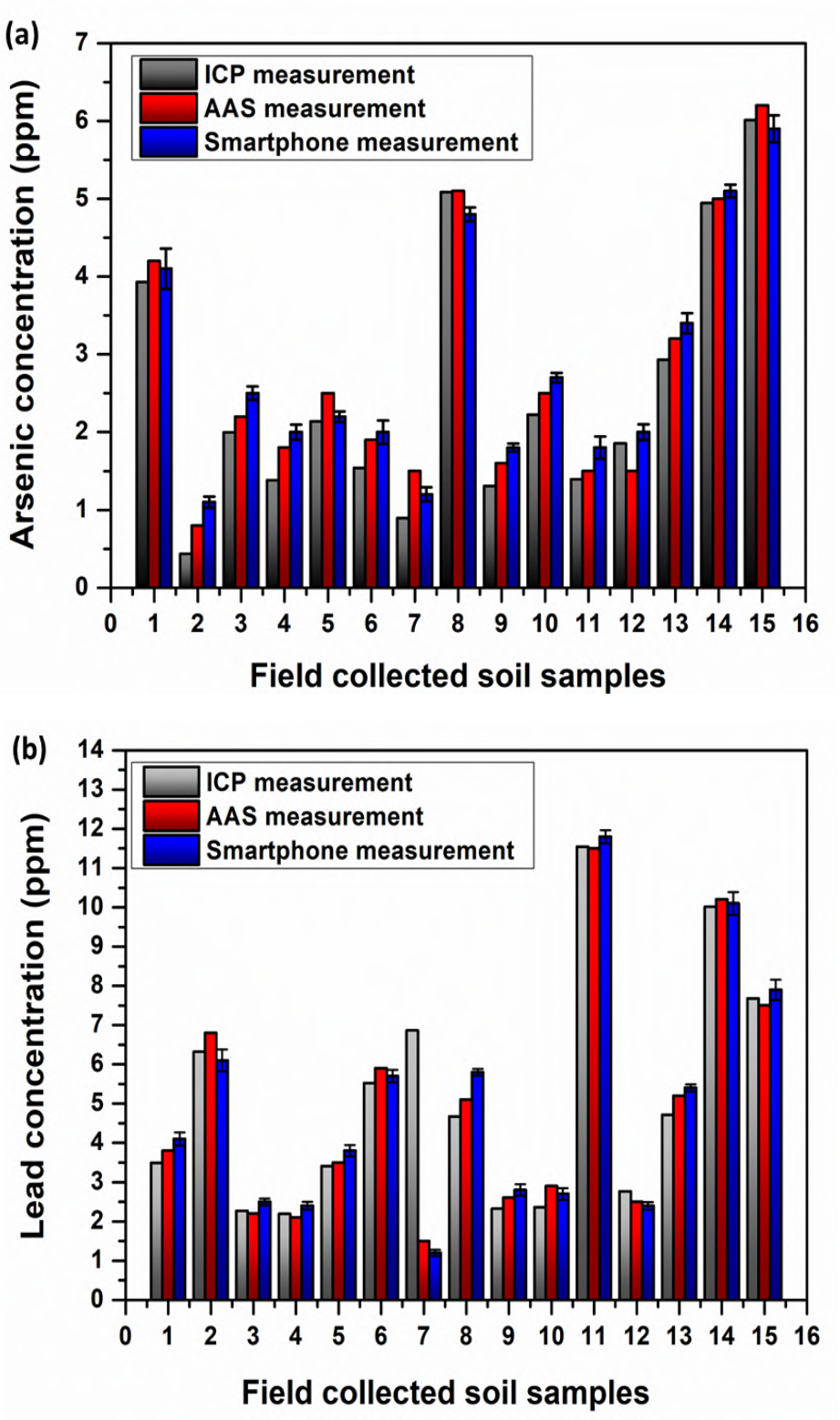

Figure 3.20: Comparative bar-graph illustration of measurements done by the atomic absorption spectrophotometer, designed smartphone-based sensor, and inductive coupled plasma spectrometer for (a) Arsenic(III) and (b) Lead(II).

for As(III) and Pb(II), respectively. For As(III) a maximum variation of 4% has been noticed between the experimental results obtained from the smartphone sensor and

the standard analytical tools, while for the Pb(III) the variation was found to be 2%. These results suggest that the designed smartphone sensor can reliably estimate these toxic metal ions As(III) and Pb(II) in soil medium.

Table 3.3 represents the As(III) and Pb(II) measurements of field-collected soil samples by standard inductive coupled spectrometer, atomic absorption spectrophotometer and designed smartphone sensor. The maximum variation in As(III) concentration measurement by the designed sensor and the standard analytical tools was found to be less than 4%, while for the Pb(III) concentration measurement the variation was found to be 2%. This obtained data suggests a good degree of reliability of the proposed tool.

3.4 Summary

In conclusion, the applicability of a smartphone has been demonstrated as a low-cost option for spectrometric sensing research that is effective for estimation of important parameters of soil. Two optical detection methods have been discussed by using a truly compact and robust smartphone based spectroscopic sensing systems. At first, smartphone's inbuilt rare camera along with optical components have been utilised to transform the device into a spectrometric platform, and its viability has been demonstrated to estimate the pH level in soil samples. The sensing system consists of a 3D printed compact optical set-up which can be attached to the smartphone's rear camera. The proposed smartphone-based spectrometric technique involves measuring the change of transmission intensity, which is correlated with the change in the sample's pH value. The performance of the device has been evaluated by comparing the pH values of field collected soil samples with a laboratory grade pH meter. Further the experimental setup of the designed sensing tool has been modified to detect toxic metal ions present in soil. The LSPR based sensing approach for selective and sensitive estimation of As(III) and Pb(II) in soil using smartphone has been demonstrated. The performance of the designed sensor has been evaluated by estimating As(III) and Pb(II) levels in agricultural soil samples and the results were found to be at par with the laboratory grade tool. The designed sensor offers other advantages like portability and data sharing ability of the sensor, thus can be used as an alternative to exiting toxic metal ion detection techniques for in-field applications. The need for an additional computational analysis system has been eliminated with the usage of custom developed android application for detection as well as analysis of the samples within the phone itself. It is envisioned that the proposed sensor could emerge as an alternative sensing tool which would facilitate common people for an easy, rapid and cost-effective soil quality analysis in the near future.

Table 3.3: Measured As(III) and Pb(II) concentration of field-collected soil samples by standard inductive coupled spectrometer, atomic absorption spectrophotometer and designed smartphone sensor.

Soil samples	**Analyte**	**ICP measurement**	**AAS measurement**	**Smartphone sensor measurement**
Sample 1	As	3.9	4.2	4.1
	pb	3.4	3.8	4.1
Sample 2	As	0.4	0.8	1.1
	pb	6.3	6.8	6.1
Sample 3	As	2.0	2.2	2.5
	pb	2.2	2.2	2.5
Sample 4	As	1.3	1.8	2.0
	pb	2.1	2.1	2.4
Sample 5	As	2.1	2.5	2.2
	pb	3.4	3.5	3.8
Sample 6	As	1.5	1.9	2.0
	pb	5.5	5.9	5.7
Sample 7	As	1.1	1.5	1.2
	pb	1.8	1.5	1.2
Sample 8	As	5.0	5.1	4.8
	pb	4.6	5.1	5.4
Sample 9	As	1.3	1.6	1.8
	pb	2.3	2.6	2.8
Sample 10	As	2.2	2.5	2.7
	pb	2.3	2.9	2.7
Sample 11	As	1.3	1.5	1.8
	pb	11.5	11.5	11.8
Sample 12	As	1.8	1.5	2.0
	pb	2.7	2.5	2.4
Sample 13	As	2.9	3.2	3.4
	pb	4.7	5.2	5.4
Sample 14	As	4.9	5.0	5.1
	pb	10.0	10.2	10.1
Sample 15	As	6.0	6.2	5.9
	pb	7.6	7.5	7.9

References

[1] Bargrizan, S., Smernik, R., and Mosley, L. Spectrophotometric measurement of the ph of soil extracts using a multiple indicator dye mixture. *European journal of soil science*, 70(2):411–420, 2019.

[2] Essington, M. E. *Soil and water chemistry: an integrative approach*. CRC press, 2015.

[3] Miller, R. O. and Kissel, D. E. Comparison of soil ph methods on soils of north america. *Soil Science Society of America Journal*, 74(1):310–316, 2010.

[4] Lindsay, W. L. et al. *Chemical equilibria in soils*. John Wiley and Sons Ltd., 1979.

[5] Kumar, S., Thakur, R., et al. Soil ph sensing techniques and technologies. *International Journal of Advanced Research in Electrical, Electronics and Instrumentation Engineering*, 4(5):1–3, 2015.

[6] Heintze, S. The use of the glass electrode in soil reaction and oxidation-reduction potential measurements. *The Journal of Agricultural Science*, 24(1):28–41, 1934.

[7] Manov, G., DeLollis, N., and Acree, S. Liquid junction potentials, and relative activity coefficients of chloride ions, in concentrated mixed chlorides and nitrates at 25° c. *J. Res. Natl. Bur. Stand*, 33:273–285, 1944.

[8] Skoog, D. A., Holler, F. J., and Crouch, S. R. *Principles of instrumental analysis*. Cengage learning, 2017.

[9] Snyder, E. F. *Methods for determining the hydrogen-ion concentration of soils*. Number 56. US Department of Agriculture, 1935.

[10] Raupach, M. and Tucker, B. The field determination of soil reaction. *Journal of the Australian Institute of Agricultural Science*, 25(2):129–133, 1959.

[11] Mouazen, A., Kuang, B., De Baerdemaeker, J., and Ramon, H. Comparison among principal component, partial least squares and back propagation neural network analyses for accuracy of measurement of selected soil properties with visible and near infrared spectroscopy. *Geoderma*, 158(1-2):23–31, 2010.

[12] Peng, X., Shi, T., Song, A., Chen, Y., and Gao, W. Estimating soil organic carbon using vis/nir spectroscopy with svmr and spa methods. *Remote Sensing*, 6(4):2699–2717, 2014.

[13] Wang, Y., Huang, T., Liu, J., Lin, Z., Li, S., Wang, R., and Ge, Y. Soil ph value, organic matter and macronutrients contents prediction using optical diffuse reflectance spectroscopy. *Computers and Electronics in Agriculture*, 111: 69–77, 2015.

[14] Nordstrom, D. K. Worldwide occurrences of arsenic in ground water.(policy forum: public health). *Science*, 296(5576):2143–2143, 2002.

[15] Patel, K., Shrivas, K., Brandt, R., Jakubowski, N., Corns, W., and Hoffmann, P. Arsenic contamination in water, soil, sediment and rice of central india. *Environmental Geochemistry and health*, 27(2):131–145, 2005.

[16] Laghari, G. N., Nafady, A., Al-Saeedi, S. I., Sherazi, S. T. H., Nisar, J., Shah, M. R., Abro, M. I., Arain, M., and Bhargava, S. K. Ranolazine-functionalized copper nanoparticles as a colorimetric sensor for trace level detection of as3+. *Nanomaterials*, 9(1):83, 2019.

[17] Gu, H., Yang, Y., Chen, F., Liu, T., Jin, J., Pan, Y., and Miao, P. Electrochemical detection of arsenic contamination based on hybridization chain reaction and recjf exonuclease-mediated amplification. *Chemical Engineering Journal*, 353:305–310, 2018.

[18] Banerjee, S., Kumar, N. P., Srinivas, A., and Roy, S. Core-shell fe3o4@ au nanocomposite as dual-functional optical probe and potential removal system for arsenic (iii) from water. *Journal of hazardous materials*, 375:216–223, 2019.

[19] Shah, T., Munsif, F., D'amato, R., and Nie, L. Lead toxicity induced phytotoxic impacts on rapeseed and clover can be lowered by biofilm forming lead tolerant bacteria. *Chemosphere*, 246:125766, 2020.

[20] Liu, S., Ni, L., Chen, W., Wang, J., and Ma, F. Analysis of lead forms and transition in agricultural soil by nano-fluorescence method. *Journal of hazardous materials*, 389:121469, 2020.

[21] Li, J., Chen, L., Lou, T., and Wang, Y. Highly sensitive sers detection of as3+ ions in aqueous media using glutathione functionalized silver nanoparticles. *ACS applied materials & interfaces*, 3(10):3936–3941, 2011.

[22] Sajed, S., Kolahdouz, M., Sadeghi, M. A., and Razavi, S. F. High-performance estimation of lead ion concentration using smartphone-based colorimetric analysis and a machine learning approach. *ACS omega*, 5(42):27675–27684, 2020.

[23] Punshon, T., Jackson, B. P., Meharg, A. A., Warczack, T., Scheckel, K., and Guerinot, M. L. Understanding arsenic dynamics in agronomic systems to predict

and prevent uptake by crop plants. *Science of the Total Environment*, 581: 209–220, 2017.

[24] Finster, M. E., Gray, K. A., and Binns, H. J. Lead levels of edibles grown in contaminated residential soils: a field survey. *Science of the Total Environment*, 320(2-3):245–257, 2004.

[25] Lloyd, D. D. Preparation of ph buffer solutions. http://delloyd.50megs.com/moreinfo/buffers2.html, Feb. 2000.

[26] Rayment, G. E. and Lyons, D. J. *Soil chemical methods: Australasia*, volume 3. CSIRO publishing, 2011.

[27] Corporation, N. Diffraction grating physics. https://www.newport.com/n/diffraction-grating-physics, Oct. 2022.

[28] Nakra, B. and Chaudhry, K. *Instrumentation, measurement and analysis*. Tata McGraw-Hill Education, 2003.

[29] Armbruster, D. A. and Pry, T. Limit of blank, limit of detection and limit of quantitation. *The clinical biochemist reviews*, 29(Suppl 1):S49, 2008.

[30] Validationof analytical procedures. http://www.ich.org/fileadmin/Public_Web_Site/ICH_Products/Guidelines/Quality/Q2_R1/Step4/Q2_R1__Guideline.pdf, 2020.

[31] Sung, Y.-M. and Wu, S.-P. Colorimetric detection of cd (ii) ions based on di-(1h-pyrrol-2-yl) methanethione functionalized gold nanoparticles. *Sensors and Actuators B: Chemical*, 201:86–91, 2014.

[32] of Technology, M. I. Mit app inventor. https://appinventor.mit.edu/explore/ai2, 2022.

[33] Shrivas, K., Sahu, B., Deb, M. K., Thakur, S. S., Sahu, S., Kurrey, R., Kant, T., Patle, T. K., and Jangde, R. Colorimetric and paper-based detection of lead using pva capped silver nanoparticles: Experimental and theoretical approach. *Microchemical Journal*, 150:104156, 2019.

[34] Wei, H., Li, B., Li, J., Dong, S., and Wang, E. Dnazyme-based colorimetric sensing of lead (pb2+) using unmodified gold nanoparticle probes. *Nanotechnology*, 19(9):095501, 2008.

[35] Kurrey, R., Deb, M. K., and Shrivas, K. Surface enhanced infra-red spectroscopy with modified silver nanoparticles (agnps) for detection of quaternary ammonium cationic surfactants. *New Journal of Chemistry*, 43(21):8109–8121, 2019.

[36] Szunerits, S. and Boukherroub, R. Sensing using localised surface plasmon resonance sensors. *Chemical Communications*, 48(72):8999–9010, 2012.

[37] Li, D. D., Gu, X., Timchenko, V., Chan, Q. N., Yuen, A. C., and Yeoh, G. H. Study of morphology and optical properties of gold nanoparticle aggregates under different ph conditions. *Langmuir*, 34(35):10340–10352, 2018.

[38] Jain, P. K. and El-Sayed, M. A. Plasmonic coupling in noble metal nanostructures. *Chemical Physics Letters*, 487(4-6):153–164, 2010.

[39] Hudson-Edwards, K., Houghton, S., and Osborn, A. Extraction and analysis of arsenic in soils and sediments. *TrAC Trends in Analytical Chemistry*, 23(10-11): 745–752, 2004.

[40] Gzar, H. A., Abdul-Hameed, A. S., and Al-Taie, A. Extraction of lead, cadmium and nickel from contaminated soil using acetic acid. *Open journal of soil science*, 4(06):207–214, 2014.